Analysis-aware defeaturing:
problem setting and *a posteriori* estimation

A. Buffa[1,2], O. Chanon[1], R. Vázquez[1,2]

[1] MNS, Institute of Mathematics, École Polytechnique Fédérale de Lausanne, Switzerland

[2] Istituto di Matematica Applicata e Tecnologie Informatiche 'E. Magenes' (CNR), Pavia, Italy

November 23, 2021

Abstract

Defeaturing consists in simplifying geometrical models by removing the geometrical features that are considered not relevant for a given simulation. Feature removal and simplification of computer-aided design models enables faster simulations for engineering analysis problems, and simplifies the meshing problem that is otherwise often unfeasible. The effects of defeaturing on the analysis are then neglected and, as of today, there are basically very few strategies to quantitatively evaluate such an impact. Understanding well the effects of this process is an important step for automatic integration of design and analysis. We formalize the process of defeaturing by understanding its effect on the solution of Poisson equation defined on the geometrical model of interest containing a single feature, with Neumann boundary conditions on the feature itself. We derive an *a posteriori* estimator of the energy error between the solutions of the exact and the defeatured geometries in $\mathbb{R}^n$, $n \in \{2, 3\}$, that is simple, reliable and efficient up to oscillations. The dependence of the estimator upon the size of the features is explicit.

Keywords: Geometric defeaturing, *a posteriori* error estimation, isogeometric analysis.
AMS Subject Classification: 65N50, 65N30

1 Introduction

Complex geometrical models are created and processed using computer-aided design tools (CAD) in the context of computer-aided engineering. The automatic integration of design and analysis tools in a single workflow has been an important topic of research for many years [1, 2]. One of the methodologies that emerged in the last 15 years is the one based on isogeometric analysis (IGA) [3, 4], a method to solve partial differential equations (PDEs) using smooth B-splines, NURBS or variances thereof as basis functions for the solution field. IGA has proven to be a valid simulation method in a wide range of applications [5], and a sound mathematical theory [6, 7], including strategies for adaptive refinement [8–11], is now available.

However, a major challenge remains in the usability of complex CAD geometries in the analysis phase. While the first CAD models used in IGA were relatively simple geometries defined by multiple patches [3, 12], in recent years, more effort is being dedicated to the analysis on complex geometries defined via Boolean operations such as intersections (trimming) [13–15] and unions [16–18]. The related engineering literature includes in particular the shell analysis on models with B-reps [19–21], and the finite cell method combined with IGA on complex geometries [22–24]. Before even doing any simulation on complex geometries, defining them may already require a very large number of degrees of freedom, that are not necessarily needed – and potentially too costly to be taken into account– to perform an accurate analysis. Moreover, repeated design changes is part of a typical process in simulation-based design for manufacturing, and it involves adding or removing geometrical features to the design, as well as adjusting geometric parameters in order to meet functionality, manufacturability and aesthetic requirements. Therefore, to be able to consider complex geometries and to accelerate the process of analysis-aware geometric design, it is essential to be able to

(a) Original geometry Ω with multiple features (fillets, holes, protrusions).

(b) Defeatured (or simplified) geometry Ω_0.
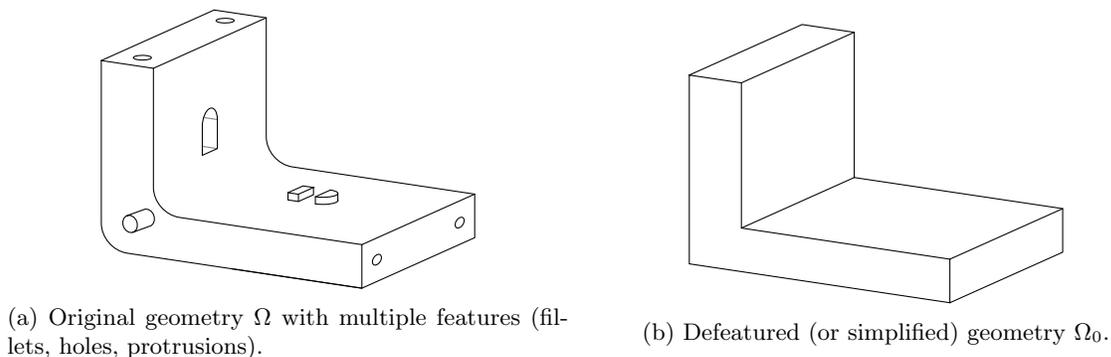
Figure 1: Illustration of defeaturing.

simplify the geometrical model, process also called defeaturing, while understanding its effect on the solution of the problem in hand. The idea of defeaturing is illustrated in Fig. 1, where we show a complex geometry and its simplified version, with all the features removed.

For a long time, the defeaturing problem has been approached using subjective *a priori* criteria, relying mostly on the engineers' expertise or based on geometrical considerations such as variations in volume or area of the domain [25]. More objective criteria have then been considered, still based on some *a priori* knowledge of the mechanical problem at hand such as the verification of constitutive or conservation laws [26, 27]. However, in order to automatize the simulation-based design process, the interest is to have an *a posteriori* criterion to assess the error introduced by defeaturing from the result of the analysis in the defeatured geometric model. Following this direction, an *a posteriori* criterion is given in Ref. [28]: it evaluates an approximation of the energy norm between the exact solution of the problem at hand and the solution on the defeatured geometry. It is intuitively based on the fact that the energy error due to defeaturing is concentrated in the modified boundaries of the geometry, and this boundary error is estimated by solving local problems around each feature. Nevertheless, this approach does not give a demonstrated certification that the proposed criterion is indeed a good estimator of the defeaturing error.

A different approach is based on the concept of feature sensitivity analysis (FSA) [29, 30], which relies on topological sensitivity analysis [31, 32], a method used in design optimization that studies the impact of infinitesimal (topological) geometrical changes on the solution of a given PDE. The works on FSA study the defeaturing in geometries with a single arbitrarily-shaped feature. First order changes of quantities of interest are analyzed when a small internal or boundary hole is removed from the geometry. However, besides the underlying assumption of infinitesimal features, this technique cannot be generalized to more complex features.

An alternative approach, still based on *a posteriori* error estimators, is proposed in Ref. [33] for internal holes. The idea behind this estimator is to reformulate the geometrical defeaturing error as a modeling error, by rewriting the PDE solved in two different geometries as two different PDEs on a unique geometry. The modeling error is then estimated using the dual weighted residual method introduced in Ref. [34] and Ref. [35], following the lines of Refs. [36–38] that study heterogeneous and perforated materials, and Ref. [39] that studies the error introduced by the approximation of boundary conditions, two problems that can be easily related to defeaturing. This a posteriori approach has then been generalized to different linear and non-linear problems, and to other types of features, in Refs. [40–43]. However, some heuristic remains in all these contributions, and a precise mathematical study of the estimator with regards to its efficiency and stability is lacking. In particular, it is assumed that the difference between the solutions of the PDE in the exact and defeatured geometries is small, and it relies on the heuristic estimation of constants that depend on the size of the features, but are not explicit with respect to it.

Consequently, the first aim of this paper is to give a solid mathematical framework for analysis-based defeaturing, and to precisely define the defeaturing error. We consider geometries that contain a single feature, the case of a geometry with multiple features being the subject of our subsequent work in preparation.

We work in the context of Poisson equation for which Neumann boundary conditions are imposed on the features, and we introduce an *a posteriori* estimator of the defeaturing error that explicitly depends on the size of the features. Our estimator is easy to compute, very cheap, and it is proven to be reliable and efficient up to oscillations. Moreover, the considered features are very general, they can either be negative (internal or boundary holes), positive (protrusions), or more complex with both positive and negative components. As mentioned earlier, the estimator is very cheap to compute: after the computation of the solution in the defeatured domain, it only requires the solution of a local problem in a simplified feature (as, e.g., its bounding box) if the feature is positive, and the computation of local boundary integrals. Indeed, the proposed estimator is derived from a representation of the defeaturing error that only involves differences between boundary terms on the feature, as already observed in Refs. [29, 30] and in Refs. [40–42].

After introducing the notation used throughout the article in Sec. 2, we precisely define the defeaturing problem in Sec. 3 in the simpler setting in which the feature is either negative or positive. Then, in Sec. 4, the defeaturing error estimator is derived and analyzed in the case in which the geometry contains a negative feature. In Sec. 5, the defeaturing problem and error estimator are generalized to the case of a geometry with a complex feature, required by complex geometric models. The study of the defeaturing problem when the feature is positive can be deduced from Sec. 5 as a special case. Subsequently, in Sec. 6, we present a validation of the results presented previously. Our validation is obtained by comparing errors and defeaturing estimators for numerical solutions on very fine meshes. We finally draw conclusions in Sec. 7, and some mathematical results used throughout the paper are stated and proven in Appendix A.

2   Notation

We start by introducing the notation that will be used throughout the paper. Let $n = 2$ or $n = 3$, let ω be any open k-dimensional manifold in $\mathbb{R}^n$, $k \leq n$, and let $\varphi \subset \partial\omega$.

We denote by $|\omega|$, $\overline{\omega}$, $\text{int}(\omega)$ and $\text{conn}(\omega)$, respectively, the measure of ω, its closure, its interior, and the set of its connected components. We also denote by $\text{diam}(\varphi)$ and $\text{hull}(\varphi)$, respectively, the manifold diameter and convex hull. More precisely, if φ is connected, we let $\text{diam}(\varphi) := \max_{\xi, \eta \in \varphi} \rho(\xi, \eta)$, where $\rho(\xi, \eta)$ is the infimum of lengths of continuous piecewise C^1-paths between ξ and η in φ. If φ is not connected, by abuse of notation, we denote by $\text{diam}(\varphi)$ the diameter of $\text{hull}(\varphi)$, where $\text{hull}(\varphi)$ is the smallest geodesically convex subset of $\partial\omega$ containing φ, that is, given any two points in $\text{hull}(\varphi)$, there is a unique minimizing geodesic contained within $\text{hull}(\varphi)$ that joins those two points.

Moreover, for any function z defined on ω, we denote $\overline{z}^{\omega}$ its average over ω. Furthermore, for $1 \leq p \leq \infty$, let $\|\cdot\|_{L^p(\omega)}$ be the norm in $L^p(\omega)$, and let $H^s(\omega)$ denote the Sobolev space of order $s \in \mathbb{R}$ whose classical norm and semi-norm are written $\|\cdot\|_{s,\omega}$ and $|\cdot|_{s,\omega}$, respectively. We recall from Ref. [44, Definition 1.3.2.1], that for all $z \in H^s(\omega)$ with $\theta := s - \lfloor s \rfloor$,

$$\|z\|_{s,\omega}^2 := \|z\|_{\lfloor s \rfloor, \omega}^2 + |z|_{\theta, \omega}^2; \qquad |z|_{\theta, \omega}^2 := \int_\omega \int_\omega \frac{\left(z(x) - z(y)\right)^2}{|x - y|^{k + 2\theta}} \, \mathrm{d}x \, \mathrm{d}y.$$

We also write $L^2(\omega) := H^0(\omega)$ so that the norm in $L^2(\omega)$ will be written $\|\cdot\|_{0,\omega}$. And to deal with boundary conditions, for $z \in H^{\frac{1}{2}}(\varphi)$, we denote

$$H^1_{z,\varphi}(\omega) := \left\{ y \in H^1(\omega) : \text{tr}_\varphi(y) = z \right\},$$

where $\text{tr}_\varphi(y)$ denotes the trace of y on $\varphi \subset \partial\omega$. Moreover, we consider the Sobolev space

$$H^{\frac{1}{2}}_{00}(\varphi) := \left\{ z \in L^2(\varphi) : z^\star \in H^{\frac{1}{2}}(\partial\omega) \right\},$$

where $z^\star$ is the extension of z by 0 on $\partial\omega$, with its norm and semi-norm that we respectively denote $\|\cdot\|_{H^{1/2}_{00}(\varphi)}$ and $|\cdot|_{H^{1/2}_{00}(\varphi)}$, where

$$\|z\|_{H^{1/2}_{00}(\varphi)}^2 := \|z\|_{\frac{1}{2}, \varphi}^2 + |z|_{H^{1/2}_{00}(\varphi)}^2 \quad \text{and} \quad |z|_{H^{1/2}_{00}(\varphi)}^2 := \int_\varphi \int_{\partial\omega \setminus \varphi} \frac{z^2(s)}{|s - t|^n} \, \mathrm{d}t \, \mathrm{d}s.$$

We recall from Ref. [44, Lemma 1.3.2.6], that there are two constants $C \geq c > 0$ (independent from the measure of φ) such that for all $z \in H_{00}^{\frac{1}{2}}(\varphi)$,

$$c|z|^2_{H_{00}^{1/2}(\varphi)} \leq \int_\varphi \frac{z^2(s)}{\text{dist}\,(s, \partial\varphi)}\,\mathrm{d}s \leq C|z|^2_{H_{00}^{1/2}(\varphi)},$$

and from Ref. [44, Eq. (1,3,2,7)], $\|z\|_{H_{00}^{1/2}(\varphi)} = \|z^\star\|_{\frac{1}{2}, \partial\omega}$. In particular, we have $|z|^2_{\frac{1}{2}, \varphi} + |z|^2_{H_{00}^{1/2}(\varphi)} = |z^\star|^2_{\frac{1}{2}, \partial\omega}$. When φ is not a connected set, then we define

$$H_{00}^{\frac{1}{2}}(\varphi) := \left\{ z \in L^2(\varphi) : z|_{\varphi_c} \in H_{00}^{\frac{1}{2}}(\varphi_c), \forall \varphi_c \in \text{conn}(\varphi) \right\},$$

and we equip this space with the norm

$$\| \cdot \|_{H_{00}^{1/2}(\varphi)} := \left(\sum_{\varphi_c \in \text{conn}(\varphi)} \| \cdot \|^2_{H_{00}^{1/2}(\varphi_c)} \right)^{\frac{1}{2}}.$$

Next, let $H_{00}^{-\frac{1}{2}}(\varphi)$ be the dual space of $H_{00}^{\frac{1}{2}}(\varphi)$ equipped with the dual norm written $\|\cdot\|_{H_{00}^{-1/2}(\varphi)}$. Furthermore, for $m \in \mathbb{N}$, let $\mathbb{Q}_m(\omega)$ be the set of polynomials on ω of degree at most m on each variable. And if $\{\omega_\ell\}_{\ell=1}^L$ is a given partition of ω such that each ω_ℓ is a flat element, that is, a straight line if $k = 1$ or a flat square or triangle if $k = 2$, let $\mathbb{Q}_{m,0}^{\text{pw}}(\omega)$ be the set of continuous functions q such that $q|_{\partial\omega} \equiv 0$, $q|_{\omega_\ell} \in \mathbb{Q}_m(\omega_\ell)$ for all $\ell = 1, \ldots, L$.

Finally, we will need the following assumptions on different domains, where the symbol $\lesssim$ is used to mean any inequality which does not depend on the size of considered domains, but which can depend on their shape.

Definition 2.1 We say that ω is *isotropic* if

$$\text{diam}\,(\omega) \lesssim \max_{\omega_c \in \text{conn}(\omega)} \left(\text{diam}(\omega_c) \right),$$

and if each connected component ω_c of ω is isotropic, that is if $\text{diam}(\omega_c)^k \lesssim |\omega_c|$, for all $\omega_c \in \text{conn}(\omega)$.

Definition 2.2 We say that ω is *regular* if ω is piecewise shape regular and composed of flat elements, that is, if there is $L_\omega \in \mathbb{N}$ such that $\omega = \text{int}\left(\bigcup_{\ell=1}^{L_\omega} \overline{\omega_\ell} \right)$, where for all $\ell, m = 1, \ldots, L_\omega$, $\omega_\ell \cap \omega_m = \emptyset$, $|\omega| \lesssim |\omega_\ell|$ and ω_ℓ is flat (for instance, if $k = 1$, it is a straight line).

If ω is regular, for all $m \in \mathbb{N}$, we define $\Pi_{m,\omega} : L^2(\omega) \rightarrow \mathbb{Q}_{m,0}^{\text{pw}}(\omega)$ as the extension of the Clément operator [45] developed in Ref. [46] on ω.

3 Defeaturing model problem

Let us consider a given open Lipschitz domain $\Omega \subset \mathbb{R}^n$ that can potentially be complex: in this paper, we assume that it contains a feature F, that is, one geometrical detail of smaller scale. There exist three kinds of such geometrical features: a feature $F \subset \mathbb{R}^n$ is said to be

- negative if $\left(\overline{F} \cap \overline{\Omega} \right) \subset \partial\Omega$;

- positive if $F \subset \Omega$;

- complex if it is composed of both negative and positive components.

(a) Domain with a negative feature.

(b) Domain with a positive feature.

(c) Simplified domain for domains (a) and (b).

(d) Domain with a positive feature, $\Omega := \operatorname{int}\left(\overline{\Omega_0} \cup \overline{F}\right)$.
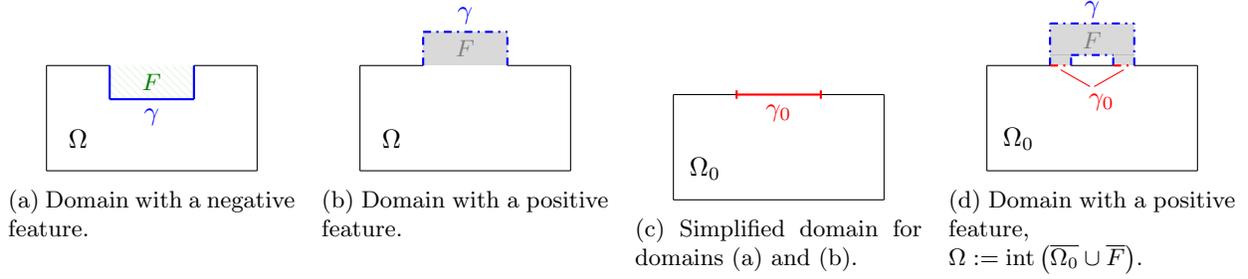
Figure 2: Different examples of geometries with a negative or a positive feature.

A positive feature corresponds to the addition of some material, a negative feature corresponds to a part where some material has been removed, and a feature is complex in the most general situation that corresponds to both the addition and the removal of some material.

In this section, we suppose that F is either negative or positive, and the considered defeaturing problem is stated, together with the notation for the problem that will be used throughout the article. The general situation in which F is a complex feature will then be studied in Sec. 5.

So for now, let F be an open Lipschitz feature which is either positive or negative, as in Fig. 2. Then, let $\Omega_0 \subset \mathbb{R}^n$ be the defeatured (or simplified) geometry, that is

- if F is negative, $\Omega_0 := \operatorname{int}\left(\overline{\Omega} \cup \overline{F}\right)$;

- if F is positive, $\Omega_0 := \Omega \setminus \overline{F}$,

and we also assume that Ω_0 is an open Lipschitz domain. In other words, if the feature F is negative, then the exact domain Ω is embedded in the defeatured domain Ω_0; if F is positive instead, the exact domain Ω is the union of the defeatured domain Ω_0 and the feature F.

Let $\mathbf{n}$, $\mathbf{n}_0$ and $\mathbf{n}_F$ be the unitary outward normals of Ω, Ω_0 and F respectively. Let $\partial\Omega = \overline{\Gamma_D} \cup \overline{\Gamma_N}$, $\Gamma_D \cap \Gamma_N = \emptyset$ with $\Gamma_D \neq \emptyset$, and we assume that $\Gamma_D \cap \partial F = \emptyset$. Finally, let $\gamma_0 := \partial F \setminus \overline{\Gamma_N} \subset \partial\Omega_0$ and $\gamma := \partial F \setminus \overline{\gamma_0} \subset \partial\Omega$ so that $\partial F = \overline{\gamma} \cup \overline{\gamma_0}$ and $\gamma \cap \gamma_0 = \emptyset$ (see Fig. 2). In particular, note that an internal feature F is a negative feature for which $\gamma = \partial F$ and $\gamma_0 = \emptyset$. In the following, the defeaturing problem is stated, and the cases in which F is either positive or negative are treated separately.

Let $h \in H^{\frac{3}{2}}(\Gamma_D)$, $g \in H^{\frac{1}{2}}(\Gamma_N)$ and $f \in L^2(\Omega)$. The considered problem is Poisson equation on the exact geometry Ω: find $u \in H^1(\Omega)$, the weak solution of

$$\begin{cases} -\Delta u = f & \text{in } \Omega \\ u = h & \text{on } \Gamma_D \\ \dfrac{\partial u}{\partial \mathbf{n}} = g & \text{on } \Gamma_N, \end{cases} \tag{1}$$

that is, $u \in H^1_{h,\Gamma_D}(\Omega)$ satisfies for all $v \in H^1_{0,\Gamma_D}(\Omega)$,

$$\int_\Omega \nabla u \cdot \nabla v \, \mathrm{d}x = \int_\Omega f v \, \mathrm{d}x + \int_{\Gamma_N} g v \, \mathrm{d}s. \tag{2}$$

If feature F is negative, consider any L^2-extension of $f \in L^2(\Omega)$ in F, that we still write $f \in L^2(\Omega_0)$ by abuse of notation. Note that such an extension is not needed for a positive feature. Then, instead of (1), the following defeatured (or simplified) problem is solved: given $g_0 \in H^{\frac{1}{2}}(\gamma_0)$, find $u_0 \in H^1(\Omega_0)$, the weak

solution of

$$\begin{cases} -\Delta u_0 = f & \text{in } \Omega_0 \\ u_0 = h & \text{on } \Gamma_D \\ \dfrac{\partial u_0}{\partial \mathbf{n}_0} = g & \text{on } \Gamma_N \setminus \gamma \\ \dfrac{\partial u_0}{\partial \mathbf{n}_0} = g_0 & \text{on } \gamma_0, \end{cases} \tag{3}$$

that is, $u_0 \in H^1_{h,\Gamma_D}(\Omega_0)$ satisfies for all $v \in H^1_{0,\Gamma_D}(\Omega_0)$,

$$\int_{\Omega_0} \nabla u_0 \cdot \nabla v \, \mathrm{d}x = \int_{\Omega_0} f v \, \mathrm{d}x + \int_{\Gamma_N \setminus \gamma} g v \, \mathrm{d}s + \int_{\gamma_0} g_0 v \, \mathrm{d}s. \tag{4}$$

We are interested in controlling the energy norm of the defeaturing error, which we suitably define in what follows.

Negative feature case: since $\Omega \subset \Omega_0$ in this case, we consider the restriction of u_0 to Ω. Then we define the defeaturing error as $\left| u - u_0 |_{\Omega} \right|_{1,\Omega}$. In this setting, we suppose that γ is isotropic according to Definition 2.1, where the diameter and the convex hull of γ are considered in the manifold $\partial\Omega$ (see Sec. 2).

Positive feature case: the solution u_0 is only defined in the defeatured geometry Ω_0 which does not contain the feature F, since $F \subset \Omega$ but $F \not\subset \Omega_0$. That is, the solution u_0 is not defined everywhere on the exact geometry $\Omega = \text{int}\left(\overline{\Omega_0 \cup F}\right)$. Therefore, to define the defeaturing error, and since Ω is the union of Ω_0 and F, one needs to solve a problem to extend u_0 to F. The most natural extension would be the solution of

$$\begin{cases} -\Delta \tilde{u}_0 = f & \text{in } F \\ \tilde{u}_0 = u_0 & \text{on } \gamma_0 \\ \dfrac{\partial \tilde{u}_0}{\partial \mathbf{n}_F} = g & \text{on } \gamma. \end{cases} \tag{5}$$

However, F may be complex or even non-smooth (see the examples in Sec. 6.3), thus finding or computing the solution of (5) may be cumbersome. Therefore, let $\tilde{F} \subset \mathbb{R}^n$ be a Lipschitz domain that contains F and such that $\gamma_0 \subset \left(\partial\tilde{F} \cap \partial F\right)$, that is, $\tilde{F}$ is a suitable (simple) domain extension of F such as the bounding box of F for example. Note that it is possible to have $\tilde{F} \cap \Omega_0 \neq \emptyset$, but we also assume that $\tilde{F} \setminus \overline{F}$ is Lipschitz. Thus if we consider any L^2-extension of f in $\tilde{F}$, that we still write f by abuse of notation, then we can solve an extension problem in $\tilde{F}$ instead of F. Note that one can look at $\tilde{F}$ as the defeatured geometry of the positive feature F, that is, as a geometry simplified from the exact geometry F, for which $\tilde{F} \setminus \overline{F}$ is a negative feature.

(a) Domain Ω with a positive feature F.

(b) Simplified domain Ω_0 and positive feature F, $\Omega = \text{int}\left(\overline{\Omega_0 \cup F}\right)$.

(c) Example of extended feature domain $\tilde{F} \supset F$.
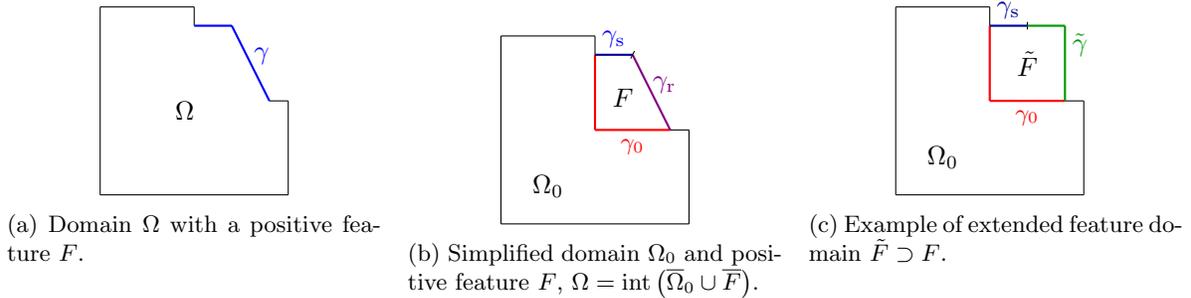
Figure 3: Example of geometry with a positive feature.

This is illustrated in Fig. 3: instead of solving the extension problem (5) in F, we can choose to solve an extension problem in $\tilde{F}$, a simpler domain which shares γ_0 as a boundary. Let $\tilde{\mathbf{n}}$ be the unitary outward normal of $\tilde{F}$, let $\tilde{\gamma} := \partial \tilde{F} \setminus \partial F$, and let γ be decomposed as $\gamma = \text{int}(\overline{\gamma_s} \cup \overline{\gamma_r})$, where γ_s and γ_r are open, γ_s is the part of γ that is shared with $\partial \tilde{F}$ while γ_r is the remaining part of γ, that is, the part that does not belong to $\partial \tilde{F}$. Note that γ_0 and $\tilde{\gamma}$ are "simple" boundaries since they are the boundaries of the chosen simplified geometry Ω_0 and of the chosen extended feature domain $\tilde{F}$, respectively.

Therefore, let us consider the following extension of the solution u_0 of (3) on $\tilde{F}$: given $\tilde{g} \in H^{\frac{1}{2}}(\tilde{\gamma})$, find $\tilde{u}_0 \in H^1\left(\tilde{F}\right)$, the weak solution of

$$\begin{cases} -\Delta \tilde{u}_0 = f & \text{in } \tilde{F} \\ \tilde{u}_0 = u_0 & \text{on } \gamma_0 \\ \dfrac{\partial \tilde{u}_0}{\partial \tilde{\mathbf{n}}} = \tilde{g} & \text{on } \tilde{\gamma} \\ \dfrac{\partial \tilde{u}_0}{\partial \tilde{\mathbf{n}}} = g & \text{on } \gamma_s, \end{cases} \tag{6}$$

that is, $\tilde{u}_0 \in H^1_{u_0, \gamma_0}\left(\tilde{F}\right)$ satisfies for all $v \in H^1_{0, \gamma_0}\left(\tilde{F}\right)$,

$$\int_{\tilde{F}} \nabla \tilde{u}_0 \cdot \nabla v \, dx = \int_{\tilde{F}} fv \, dx + \int_{\tilde{\gamma}} \tilde{g}v \, ds + \int_{\gamma_s} gv \, ds.$$

Let $u_d \in H^1_{h, \Gamma_D}(\Omega)$ be the extended defeatured solution, that is,

$$u_d = u_0 \text{ in } \Omega_0 \quad \text{and} \quad u_d = \tilde{u}_0|_{F_p} \text{ in } F_p.$$

Then we define the defeaturing error as $|u - u_d|_{1,\Omega}$.

In this setting, we suppose that γ_0 and γ_r are isotropic according to Definition 2.1, where the diameter and the convex hull γ_0 are considered in the manifold $\partial \Omega_0$, and the diameter and the convex hull of γ_r are considered in the manifold ∂F.

Remark 3.1 The problem is studied in the case in which all domains are Lipschitz, and under the isotropy conditions stated above. A finer analysis could be performed to take into account more general geometries, such as the non-Lipschitz fillet of Sec. 6.3, but this goes beyond the scope of this paper. Moreover, when used, the regularity condition defined in Definition 2.2 is taken for the sake of simplicity, but it can be relaxed by considering ω piecewise smooth and shape regular instead.

Note that the boundaries γ, γ_0 and γ_r can be non-connected sub-manifolds (see Fig. 2d). In the remaining part of this article, the symbol $\lesssim$ will be used to mean any inequality which does not depend on the size of the feature F nor on the size of the positive extension $\tilde{F}$, but which can depend on their shape. Moreover, we will write $A \simeq B$ whenever $A \lesssim B$ and $B \lesssim A$.

4 Negative feature *a posteriori* defeaturing error estimator

In this section, an optimal *a posteriori* defeaturing error estimator is derived in the simplest setting of a negative feature. We show that the derived estimator is an upper bound and a lower bound (up to oscillations) of the energy norm of the defeaturing error. The key issue in the subsequent analysis is to track the dependence of all constants from the size of the feature. Although it would be possible to present the equivalent analysis for a positive feature, we have decided to omit it and to let the positive feature case be a consequence of the more general case of a complex feature, whose dedicated analysis is presented in Sec. 5.

Let F be a negative feature of Ω, and suppose that γ is isotropic according to Definition 2.1. Then, let

$$d_\gamma := g + \frac{\partial u_0}{\partial \mathbf{n}_F} \text{ on } \gamma \tag{7}$$

be the error term on the Neumann data on γ, and we define the defeaturing error estimator as

$$\mathcal{E}_{\mathrm{n}}(u_0) := \left(|\gamma|^{\frac{1}{n-1}} \left\| d_\gamma - \overline{d_\gamma}^\gamma \right\|_{0,\gamma}^2 + c_\gamma^2 |\gamma|^{\frac{n}{n-1}} \left| \overline{d_\gamma}^\gamma \right|^2 \right)^{\frac{1}{2}}, \tag{8}$$

where, if we define $\eta \in \mathbb{R}$ as the unique solution of $\eta = -\log(\eta)$,

$$c_\gamma := \begin{cases} \max\left(|\log(|\gamma|)|, \eta \right)^{\frac{1}{2}} & \text{if } n = 2 \\ 1 & \text{if } n = 3. \end{cases} \tag{9}$$

We first show that the quantity $\mathcal{E}_{\mathrm{n}}(u_0)$ is a reliable estimator for the defeaturing error, i.e., it is an upper bound for the defeaturing error (see Theorem 4.3). Then, assuming that γ is also regular according to Definition 2.2, and under mild assumptions for the two-dimensional case, we show that it is also efficient (up to oscillations), i.e., it is a lower bound for the defeaturing error up to oscillations (see Theorem 4.4). This means that the whole information on the error introduced by defeaturing a negative feature, in energy norm, is contained in the boundary γ, and can be accounted by suitably evaluating the error made on the normal derivative of the solution.

Remark 4.1 Consider the simplified problem (3) restricted to F with the natural Neumann boundary condition on γ, that is, $u_0|_F \in H^1(F)$ satisfies

$$\begin{cases} -\Delta \left(u_0|_F \right) = f & \text{in } F \\ \dfrac{\partial \left(u_0|_F \right)}{\partial \mathbf{n}_0} = g_0 & \text{on } \gamma_0 \\ \dfrac{\partial \left(u_0|_F \right)}{\partial \mathbf{n}_F} = \dfrac{\partial u_0}{\partial \mathbf{n}_F} & \text{on } \gamma. \end{cases}$$

By abuse of notation, we omit the explicit restriction of u_0 to F. Then if we multiply the restricted problem by the constant function 1 and integrate by parts, we obtain

$$\int_F f \, \mathrm{d}x + \int_{\gamma_0} g_0 \, \mathrm{d}s + \int_\gamma \frac{\partial u_0}{\partial \mathbf{n}_F} = 0.$$

Consequently,

$$\overline{d_\gamma}^\gamma = \overline{\left(g + \frac{\partial u_0}{\partial \mathbf{n}_F} \right)}^\gamma = \frac{1}{|\gamma|} \left(\int_\gamma g \, \mathrm{d}s - \int_{\gamma_0} g_0 \, \mathrm{d}s - \int_F f \, \mathrm{d}x \right).$$

Therefore, the second term of the estimator $\mathcal{E}_{\mathrm{n}}(u_0)$ in (8) only depends on the defeatured problem data, and more precisely on the choice of g_0 that one considers on γ_0, and on the choice of the extension of f that one considers in the feature F. As a consequence, if the second term of the estimator (8) dominates, this means that the defeatured problem data should be better chosen. Moreover, under the following reasonable flux conservation assumption

$$\int_\gamma g \, \mathrm{d}s - \int_{\gamma_0} g_0 \, \mathrm{d}s - \int_F f \, \mathrm{d}x = 0, \tag{10}$$

the defeaturing error estimator (8) rewrites

$$\mathcal{E}_{\mathrm{n}}(u_0) = |\gamma|^{\frac{1}{2(n-1)}} \left\| d_\gamma \right\|_{0,\gamma}.$$

Note that condition (10) is easily met if the Neumann boundary condition g and the source function f are zero in the vicinity of the feature.

Remark 4.2 Since $(4c_\gamma^2 - 1) > 0$ for all γ, remark that by Cauchy-Schwarz inequality,

$$
\begin{aligned}
\mathcal{E}_{\mathrm{n}}(u_0) &\lesssim |\gamma|^{\frac{1}{2(n-1)}} \left[\|d_\gamma - \overline{d_\gamma}^\gamma\|_{0,\gamma}^2 + 4c_\gamma^2 |\gamma| \left(\overline{d_\gamma}^\gamma\right)^2 \right]^{\frac{1}{2}} \\
&= |\gamma|^{\frac{1}{2(n-1)}} \left[\|d_\gamma\|_{0,\gamma}^2 + \left(4c_\gamma^2 - 1\right) |\gamma| \left(\overline{d_\gamma}^\gamma\right)^2 \right]^{\frac{1}{2}} \\
&\lesssim c_\gamma |\gamma|^{\frac{1}{2(n-1)}} \|d_\gamma\|_{0,\gamma} =: \tilde{\mathcal{E}}_{\mathrm{n}}(u_0).
\end{aligned}
$$

One could be tempted to use the simpler indicator $\tilde{\mathcal{E}}_{\mathrm{n}}(u_0)$, but when $n = 2$ and under the flux conservation condition (10), $\tilde{\mathcal{E}}_{\mathrm{n}}(u_0)$ is sub-optimal since in this case, $\tilde{\mathcal{E}}_{\mathrm{n}}(u_0) = c_\gamma \mathcal{E}_{\mathrm{n}}(u_0)$. Indeed, no lower bound can be provided for $\tilde{\mathcal{E}}_{\mathrm{n}}(u_0)$.

4.1   Upper bound

In this section, we prove that the error indicator defined in (8) is reliable, that is, it is an upper bound for the defeaturing error.

Theorem 4.3 *Let u and u_0 be the weak solutions of problems (1) and (3), respectively. If γ is isotropic according to Definition 2.1, then the defeaturing error in energy norm is bounded in terms of the estimator $\mathcal{E}_{\mathrm{n}}(u_0)$ introduced in (8) as follows:*

$$
\left| u - u_0 \right|_\Omega \big|_{1,\Omega} \lesssim \mathcal{E}_{\mathrm{n}}(u_0).
$$

Proof. Let us first consider the simplified problem (3) restricted to Ω with the natural Neumann boundary condition on γ, that is, since $\mathbf{n}_F = -\mathbf{n}$ on γ, the restriction $u_0|_\Omega \in H^1_{h,\Gamma_D}(\Omega)$ is the weak solution of

$$
\begin{cases}
-\Delta\left(u_0|_\Omega\right) = f & \text{in } \Omega \\
u_0|_\Omega = h & \text{on } \Gamma_D \\
\dfrac{\partial\left(u_0|_\Omega\right)}{\partial \mathbf{n}} = g & \text{on } \Gamma_N \setminus \gamma \\
\dfrac{\partial\left(u_0|_\Omega\right)}{\partial \mathbf{n}} = -\dfrac{\partial u_0}{\partial \mathbf{n}_F} & \text{on } \gamma.
\end{cases}
\tag{11}
$$

By abuse of notation, we omit the explicit restriction of u_0 to Ω. Then, for all $v \in H^1_{0,\Gamma_D}(\Omega)$,

$$
\int_\Omega \nabla u_0 \cdot \nabla v \, \mathrm{d}x = \int_\Omega f v \, \mathrm{d}x + \int_{\Gamma_N \setminus \gamma} g v \, \mathrm{d}s - \int_\gamma \frac{\partial u_0}{\partial \mathbf{n}_F} v \, \mathrm{d}s.
\tag{12}
$$

Let $e := u - u_0 \in H^1_{0,\Gamma_D}(\Omega)$. Then for all $v \in H^1_{0,\Gamma_D}(\Omega)$, it holds from equations (2) and (12) that

$$
\begin{aligned}
\int_\Omega \nabla e \cdot \nabla v \, \mathrm{d}x &= \int_{\Gamma_N} g v \, \mathrm{d}s - \int_{\Gamma_N \setminus \gamma} g v \, \mathrm{d}s + \int_\gamma \frac{\partial u_0}{\partial \mathbf{n}_F} v \, \mathrm{d}s \\
&= \int_\gamma \left(g + \frac{\partial u_0}{\partial \mathbf{n}_F} \right) v \, \mathrm{d}s = \int_\gamma d_\gamma v \, \mathrm{d}s.
\end{aligned}
\tag{13}
$$

Now, if we take $v = e \in H^1_{0,\Gamma_D}(\Omega)$ in (13), then

$$
|e|_{1,\Omega}^2 = \int_\gamma d_\gamma e \, \mathrm{d}s = \int_\gamma \left(d_\gamma - \overline{d_\gamma}^\gamma \right) e \, \mathrm{d}s + \overline{d_\gamma}^\gamma \int_\gamma e \, \mathrm{d}s.
\tag{14}
$$

Let us first estimate the first term of (14). Thanks to Poincaré inequality of Appendix A.1 and a trace inequality,

$$
\int_\gamma \left(d_\gamma - \overline{d_\gamma}^\gamma\right) e \, ds = \int_\gamma \left(d_\gamma - \overline{d_\gamma}^\gamma\right)(e - \overline{e}^\gamma) \, ds \le \left\|d_\gamma - \overline{d_\gamma}^\gamma\right\|_{0,\gamma} \|e - \overline{e}^\gamma\|_{0,\gamma}
$$
$$
\lesssim \left\|d_\gamma - \overline{d_\gamma}^\gamma\right\|_{0,\gamma} |\gamma|^{\frac{1}{2(n-1)}} |e|_{\frac{1}{2},\gamma} \le |\gamma|^{\frac{1}{2(n-1)}} \left\|d_\gamma - \overline{d_\gamma}^\gamma\right\|_{0,\gamma} |e|_{\frac{1}{2},\partial\Omega}
$$
$$
\lesssim |\gamma|^{\frac{1}{2(n-1)}} \left\|d_\gamma - \overline{d_\gamma}^\gamma\right\|_{0,\gamma} |e|_{1,\Omega}. \tag{15}
$$

Moreover, the second term of (14) can be estimated thanks to Appendix A.2 and a trace inequality, that is,

$$
\overline{d_\gamma}^\gamma \int_\gamma e \, ds \le \left|\overline{d_\gamma}^\gamma\right| |\gamma|^{\frac{1}{2}} \|e\|_{0,\gamma} \lesssim \left|\overline{d_\gamma}^\gamma\right| c_\gamma |\gamma|^{\frac{1}{2(n-1)} + \frac{1}{2}} \|e\|_{\frac{1}{2},\partial\Omega}
$$
$$
\lesssim c_\gamma |\gamma|^{\frac{n}{2(n-1)}} \left|\overline{d_\gamma}^\gamma\right| |e|_{1,\Omega}. \tag{16}
$$

Therefore, combining (14), (15) and (16), and simplifying on both sides, we obtain the desired result. $\qquad\square$

4.2 Lower bound

In this section, we prove that the error indicator defined in (8) is efficient, that is, it is a lower bound for the defeaturing error, up to oscillations. In the case $n = 2$, the flux conservation assumption (10) is also required.

Theorem 4.4 *Let u and u_0 be as in Theorem 4.3, and assume that γ is isotropic and regular according to Definitions 2.1 and 2.2. Suppose that either $n = 3$, or $n = 2$ and the flux conservation condition (10) is satisfied. Then the defeaturing error, in energy norm, bounds up to oscillations the estimator $\mathcal{E}_n(u_0)$ introduced in (8), that is*

$$
\mathcal{E}_n(u_0) \lesssim \left|u - u_0|_\Omega\right|_{1,\Omega} + \text{osc}_n(u_0),
$$

where

$$
\text{osc}_n(u_0) := |\gamma|^{\frac{1}{2(n-1)}} \|d_\gamma - \Pi_m(d_\gamma)\|_{0,\gamma} \tag{17}
$$

for any $m \in \mathbb{N}$, with $\Pi_m := \Pi_{m,\gamma}$ being the extension of the Clément operator defined in Sec. 2.

Proof. To simplify the notation, we omit to explicitly write the restriction of u_0 to Ω when it would be necessary, since the context makes it clear. As before, let $e := u - u_0 \in H^1_{0,\Gamma_D}(\Omega)$. From equation (13), for all $v \in H^1_{0,\Gamma_D}(\Omega)$,

$$
\int_\gamma d_\gamma v \, ds = \int_\Omega \nabla e \cdot \nabla v \, dx \le |e|_{1,\Omega} |v|_{1,\Omega}. \tag{18}
$$

Now, for all $w \in H^{\frac{1}{2}}_{00}(\gamma)$, let $u_w \in H^1_{0,\partial\Omega\setminus\gamma}(\Omega) \subset H^1_{0,\Gamma_D}(\Omega)$ be the unique weak solution of

$$
\begin{cases} -\Delta u_w = 0 & \text{in } \Omega \\ u_w = w^\star & \text{on } \partial\Omega, \end{cases}
$$

where $w^\star$ is the extension of w by 0. Then $|u_w|_{1,\Omega} \lesssim \|w^\star\|_{\frac{1}{2},\partial\Omega} = \|w\|_{H^{1/2}_{00}(\gamma)}$ by continuity of the solution on the data. Therefore, using (18),

$$
\|d_\gamma\|_{H^{-1/2}_{00}(\gamma)} = \sup_{\substack{w \in H^{1/2}_{00}(\gamma) \\ w \ne 0}} \frac{\int_\gamma d_\gamma w \, ds}{\|w\|_{H^{1/2}_{00}(\gamma)}} \lesssim \sup_{\substack{w \in H^{1/2}_{00}(\gamma) \\ w \ne 0}} \frac{\int_\gamma d_\gamma u_w \, ds}{|u_w|_{1,\Omega}}
$$
$$
\le \sup_{\substack{v \in H^1_{0,\Gamma_D}(\Omega) \\ v \ne 0}} \frac{\int_\gamma d_\gamma v \, ds}{|v|_{1,\Omega}} \le \sup_{\substack{v \in H^1_{0,\Gamma_D}(\Omega) \\ v \ne 0}} \frac{|e|_{1,\Omega} |v|_{1,\Omega}}{|v|_{1,\Omega}} = |e|_{1,\Omega}. \tag{19}
$$

Moreover, using Remark 4.2 if $n = 3$, or Remark 4.1 if $n = 2$ and if the flux conservation condition (10) is satisfied, then

$$\mathcal{E}_n(u_0) \lesssim |\gamma|^{\frac{1}{2(n-1)}} \|d_\gamma\|_{0,\gamma}.$$

Therefore, using the triangle inequality and applying the inverse inequality of Appendix A.5, we get

$$\mathcal{E}_n(u_0) \lesssim |\gamma|^{\frac{1}{2(n-1)}} \left(\|\Pi_m(d_\gamma)\|_{0,\gamma} + \|d_\gamma - \Pi_m(d_\gamma)\|_{0,\gamma} \right)$$
$$\lesssim \|\Pi_m(d_\gamma)\|_{H_{00}^{-1/2}(\gamma)} + |\gamma|^{\frac{1}{2(n-1)}} \|d_\gamma - \Pi_m(d_\gamma)\|_{0,\gamma}. \tag{20}$$

Finally, using another time the triangle inequality, Appendix A.4 and (19), we obtain

$$\|\Pi_m(d_\gamma)\|_{H_{00}^{-1/2}(\gamma)} \le \|d_\gamma\|_{H_{00}^{-1/2}(\gamma)} + \|\Pi_m(d_\gamma) - d_\gamma\|_{H_{00}^{-1/2}(\gamma)}$$
$$\lesssim |e|_{1,\Omega} + |\gamma|^{\frac{1}{2(n-1)}} \|d_\gamma - \Pi_m(d_\gamma)\|_{0,\gamma}. \tag{21}$$

Consequently, combining (20) and (21), and recalling the definition (17) of the oscillations, then

$$\mathcal{E}_n(u_0) \lesssim |e|_{1,\Omega} + \mathrm{osc}_n(u_0).$$

$\square$

Remark 4.5 In some sense, the oscillations pollute the lower bound in Theorem 4.4. It is therefore important to make sure that the oscillations are asymptotically smaller than the defeaturing error, with respect to the size of the feature. While there is a strong numerical evidence of it (see Sec. 6), an *a priori* error analysis of the defeaturing problem is needed in order to obtain a rigorous proof, but this goes beyond the scope of this paper. However, we are expecting the term $\|d_\gamma\|_{0,\gamma}$ to depend on the measure of γ. When the data is regular, so is u_0, and it is then always possible to choose m large enough so that the asymptotic behavior of the oscillations is $\mathcal{O}\left(|\gamma|^{m+\frac{1}{2(n-1)}}\right)$. Therefore, upon a wise choice of m, the oscillations converge faster than the defeaturing error with respect to the measure of γ.

5 Defeaturing a geometry with a complex feature

In this section, instead of discussing only a defeaturing error estimator for a geometry containing a positive feature, we directly generalize the previous study to a geometry containing a complex feature, that is, a feature containing both negative and positive components. More precisely, we first generalize the defeaturing problem of Sec. 3 to this context, and then we derive a corresponding optimal *a posteriori* defeaturing error estimator. Building upon the study of Sec. 4, we show that the derived estimator is an upper bound and a lower bound (up to oscillations) of the energy norm of the defeaturing error, by accurately tracking the dependence of all constants from the size of the feature.

5.1 Defeaturing model problem for a complex feature

Suppose now that $F \subset \mathbb{R}^n$ is a complex feature. More precisely, this means that we suppose that F is an open Lipschitz domain which is composed of a negative component F_n and a positive component F_p that can have a non-empty intersection (see Fig. 4). More precisely, $F = \mathrm{int}\left(\overline{F_n} \cup \overline{F_p}\right)$, where F_n and F_p are open Lipschitz domains such that if we let

$$\Omega^\star := \Omega \setminus \overline{F_p},$$

then $F_p \subset \Omega$ and $\overline{F_n} \cap \overline{\Omega^\star} \subset \partial\Omega^\star$. In particular, note that if $F_p = \emptyset$ and $F = F_n$, then F is negative, while if $F_n = \emptyset$ and $F = F_p$, then F is positive, as defined in Sec. 3.

In this setting, the defeatured geometry is defined by $\Omega_0 := \mathrm{int}\left(\overline{\Omega^\star} \cup \overline{F_n}\right) \subset \mathbb{R}^n$, and as before, we also assume that Ω_0 is an open Lipschitz domain. Note that it is in general not true that $\Omega^\star = \Omega \cap \Omega_0$ (see Fig. 4f), while it is true if F is completely negative or positive.

(a) Domain with a negative feature.

(b) Domain with a positive feature.

(c) Domain with a general complex feature.

(d) Simplified domain for domains (a)–(c), (e)–(f).

(e) Domain with a general complex feature.

(f) Domain with a general complex feature.

(g) Simplified domain for domains (e), (f).

(h) Domain with a positive feature, $\Omega := \mathrm{int}\left(\overline{\Omega_0} \cup \overline{F}\right)$.
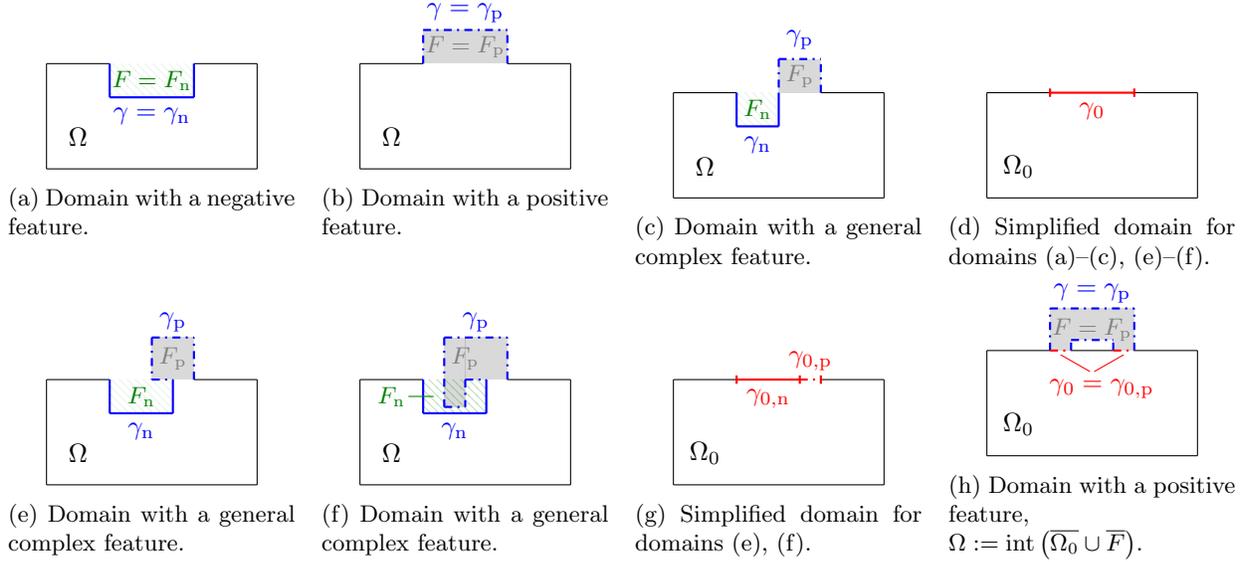
Figure 4: Different examples of geometries with a negative, a positive, or a general complex feature.

The considered problem in the exact geometry Ω is still the Poisson equation defined in (1), for which we assume that $\Gamma_D \cap (\partial F_\mathrm{n} \cup \partial F_\mathrm{p}) = \emptyset$. Moreover, let

$$\gamma_0 := \mathrm{int}\left(\overline{\gamma_{0,\mathrm{n}}} \cup \overline{\gamma_{0,\mathrm{p}}}\right) \subset \partial\Omega_0 \quad \text{with} \quad \gamma_{0,\mathrm{n}} := \partial F_\mathrm{n} \setminus \partial\Omega^\star, \quad \gamma_{0,\mathrm{p}} := \partial F_\mathrm{p} \setminus \partial\Omega,$$
$$\gamma := \mathrm{int}\left(\overline{\gamma_\mathrm{n}} \cup \overline{\gamma_\mathrm{p}}\right) \subset \partial\Omega \quad \text{with} \quad \gamma_\mathrm{n} := \partial F_\mathrm{n} \setminus \overline{\gamma_{0,\mathrm{n}}}, \quad \gamma_\mathrm{p} := \partial F_\mathrm{p} \setminus \overline{\gamma_{0,\mathrm{p}}}.$$

so that $\partial F_\mathrm{n} = \overline{\gamma_\mathrm{n}} \cup \overline{\gamma_{0,\mathrm{n}}}$ with $\gamma_\mathrm{n} \cap \gamma_{0,\mathrm{n}} = \emptyset$, and $\partial F_\mathrm{p} = \overline{\gamma_\mathrm{p}} \cup \overline{\gamma_{0,\mathrm{p}}}$ with $\gamma_\mathrm{p} \cap \gamma_{0,\mathrm{p}} = \emptyset$ (see Fig. 4).

Similarly to the negative feature case, consider any L^2-extension of the restriction $f|_{\Omega^\star}$ in the negative component F_n of F, that we still write $f \in L^2(\Omega_0)$ by abuse of notation. Then instead of (1), we solve the defeatured (or simplified) problem (3) whose weak formulation is given in (4). As previously, we are interested in controlling the energy norm of the defeaturing error, which we suitably define in what follows.

Similarly to the positive feature case, the solution u_0 of the defeatured problem is not defined everywhere on Ω since $F_\mathrm{p} \setminus \overline{F_\mathrm{n}} \not\subset \Omega_0$ but $F_\mathrm{p} \setminus \overline{F_\mathrm{n}} \subset \Omega$. Therefore, following the same rationale for F_p as the one exposed in Sec. 3, let $\tilde{F}_\mathrm{p} \subset \mathbb{R}^n$ be a Lipschitz domain that contains F_p and such that $\gamma_{0,\mathrm{p}} \subset \left(\partial\tilde{F}_\mathrm{p} \cap \partial F_\mathrm{p}\right)$, that is, $\tilde{F}_\mathrm{p}$ is a suitable (simple) domain extension of F_p such as the bounding box of F_p for example. Let us also assume that $\tilde{F}_\mathrm{p} \setminus \overline{F_\mathrm{p}}$ is Lipschitz, and consider any L^2-extension of f in $\tilde{F}_\mathrm{p}$, that we still write f by abuse of notation. Let $\tilde{\mathbf{n}}$ be the unitary outward normal of $\tilde{F}_\mathrm{p}$, let $\tilde{\gamma} := \partial\tilde{F}_\mathrm{p} \setminus \partial F_\mathrm{p}$, and let γ_p be decomposed as $\gamma_\mathrm{p} = \mathrm{int}(\overline{\gamma_\mathrm{s}} \cup \overline{\gamma_\mathrm{r}})$, where γ_s and γ_r are open, γ_s is the part of γ_p that is shared with $\partial\tilde{F}_\mathrm{p}$ while γ_r is the remaining part of γ_p, that is, the part that does not belong to $\partial\tilde{F}_\mathrm{p}$, see Fig. 5.

Therefore, and as for the positive feature case, we can consider the extension of the solution u_0 of (3) on $\tilde{F}_\mathrm{p}$, called $\tilde{u}_0 \in H^1_{u_0,\gamma_{0,\mathrm{p}}}\left(\tilde{F}_\mathrm{p}\right)$ and defined as the weak solution of (6) where F, $\tilde{F}$ and γ_0 are replaced by F_p, $\tilde{F}_\mathrm{p}$ and $\gamma_{0,\mathrm{p}}$, respectively. Now, we can define the extended defeatured solution $u_\mathrm{d} \in H^1_{h,\Gamma_D}(\Omega)$ as

$$u_\mathrm{d} = u_0|_{\Omega_0 \setminus \overline{F_\mathrm{n}}} \text{ in } \Omega^\star = \Omega \setminus \overline{F_\mathrm{p}} \quad \text{and} \quad u_\mathrm{d} = \tilde{u}_0|_{F_\mathrm{p}} \text{ in } F_\mathrm{p}. \tag{22}$$

Then the defeaturing error is defined by $|u - u_\mathrm{d}|_{1,\Omega}$.

Remark 5.1 Note that if $F_\mathrm{n} \cap F_\mathrm{p} \neq \emptyset$, it may happen that $u_0 \neq \tilde{u}_0$ on $F_\mathrm{n} \cap F_\mathrm{p}$. But in this case, on $F_\mathrm{n} \cap F_\mathrm{p}$, the definition of u_d in (22) specifies that $u_\mathrm{d} = \tilde{u}_0$.
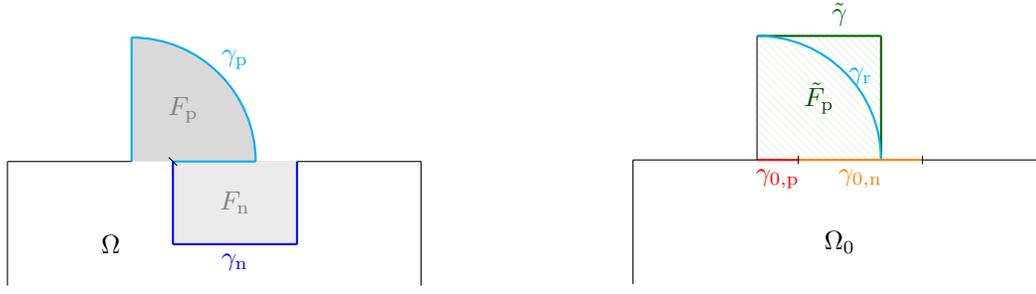
(a) Domain Ω with feature F that has non-empty positive and negative components F_p and F_n.

(b) Simplified domain Ω_0, extension $\tilde{F}_\mathrm{p}$ of the positive component of the feature, and different boundaries.

Figure 5: Example of a geometry with a feature whose positive and negative components share a part of the boundary.

In this setting, we suppose that γ_n, $\gamma_{0,\mathrm{p}}$ and γ_r are isotropic according to Definition 2.1, where the diameter and the convex hull of γ_n, $\gamma_{0,\mathrm{p}}$ and γ_r are considered in the manifolds $\partial\Omega$, $\partial\Omega_0$ and ∂F, respectively (see Sec. 2). Note that, as before, the considered boundaries can be non-connected sub-manifolds. Finally, for further use, let $\Sigma := \{\gamma_\mathrm{n}, \gamma_\mathrm{r}, \gamma_{0,\mathrm{p}}\}$ and let d_Σ be defined piecewise as $d_\Sigma|_\sigma := d_\sigma$ for all $\sigma \in \Sigma$, with

$$d_\sigma := \begin{cases} g - \dfrac{\partial u_\mathrm{d}}{\partial \mathbf{n}} & \text{if } \sigma = \gamma_\mathrm{n} \text{ or } \sigma = \gamma_\mathrm{r} \\ -\left(g_0 + \dfrac{\partial u_\mathrm{d}}{\partial \mathbf{n}_F}\right) & \text{if } \sigma = \gamma_{0,\mathrm{p}}. \end{cases} \tag{23}$$

That is, d_σ is the error term on the Neumann data for $\sigma = \gamma_\mathrm{n}$ or $\sigma = \gamma_\mathrm{r}$, and $d_{\gamma_{0,\mathrm{p}}}$ is the jump in the normal derivative of u_d due to the Dirichlet extension of u_d in the positive component of the feature.

5.2 Complex feature *a posteriori* defeaturing error estimator

Recalling the definition of the defeaturing solution u_d in (22) and of Σ and d_σ in (23), we define the defeaturing error estimator as

$$\mathcal{E}(u_\mathrm{d}) := \left[\sum_{\sigma \in \Sigma} \left(|\sigma|^{\frac{1}{n-1}} \left\|d_\sigma - \overline{d_\sigma}^\sigma\right\|_{0,\sigma}^2 + c_\sigma^2 |\sigma|^{\frac{n}{n-1}} \left|\overline{d_\sigma}^\sigma\right|^2\right)\right]^{\frac{1}{2}}, \tag{24}$$

where c_σ is defined as in (9).

Remark 5.2 If F is a negative feature, then $\mathcal{E}(u_\mathrm{d}) = \mathcal{E}_\mathrm{n}(u_0)$ where $\mathcal{E}_\mathrm{n}(u_0)$ is defined in (8), while if F is a positive feature, then $\mathcal{E}(u_\mathrm{d}) = \mathcal{E}_\mathrm{p}(\tilde{u}_0)$ where

$$\begin{aligned} \mathcal{E}_\mathrm{p}(\tilde{u}_0) := \Bigg(& |\gamma_0|^{\frac{1}{n-1}} \left\|\left(g_0 + \frac{\partial \tilde{u}_0}{\partial \mathbf{n}_F}\right) - \overline{\left(g_0 + \frac{\partial \tilde{u}_0}{\partial \mathbf{n}_F}\right)}^{\gamma_0}\right\|_{0,\gamma_0}^2 \\ & + |\gamma_\mathrm{r}|^{\frac{1}{n-1}} \left\|\left(g - \frac{\partial \tilde{u}_0}{\partial \mathbf{n}_F}\right) - \overline{\left(g - \frac{\partial \tilde{u}_0}{\partial \mathbf{n}_F}\right)}^{\gamma_\mathrm{r}}\right\|_{0,\gamma_\mathrm{r}}^2 \\ & + c_{\gamma_0}^2 |\gamma_0|^{\frac{n}{n-1}} \left|\overline{\left(g_0 + \frac{\partial \tilde{u}_0}{\partial \mathbf{n}_F}\right)}^{\gamma_0}\right|^2 + c_{\gamma_\mathrm{r}}^2 |\gamma_\mathrm{r}|^{\frac{n}{n-1}} \left|\overline{\left(g - \frac{\partial \tilde{u}_0}{\partial \mathbf{n}_F}\right)}^{\gamma_\mathrm{r}}\right|^2 \Bigg)^{\frac{1}{2}}. \end{aligned}$$

In this section, we first show that the quantity $\mathcal{E}(u_{\mathrm{d}})$ is a reliable estimator for the defeaturing error, i.e., it is an upper bound for the defeaturing error (see Theorem 5.5). Then, assuming that γ_{n}, γ_{r} and $\gamma_{0,\mathrm{p}}$ are also regular according to Definition 2.2, and under mild assumptions for the two-dimensional case, we show that it is also efficient (up to oscillations), i.e., it is a lower bound for the defeaturing error up to oscillations (see Theorem 5.6).

Remark 5.3 Consider the simplified extended problem (6) restricted to F_{p} and then to $\tilde{F}_{\mathrm{p}} \setminus F_{\mathrm{p}}$, with the natural Neumann boundary condition on $\gamma_{0,\mathrm{p}}$ and γ_{r} respectively, in a similar way to (11). By abuse of notation and as previously, we omit the explicit restriction of $\tilde{u}_0$ to F_{p} or to $\tilde{F}_{\mathrm{p}} \setminus F_{\mathrm{p}}$. Then if we multiply the restricted problems by the constant function 1 and integrate by parts, we obtain

$$\int_{F_{\mathrm{p}}} f \, \mathrm{d}x + \int_{\gamma_{\mathrm{p}}} g \, \mathrm{d}s + \int_{\gamma_{0,\mathrm{p}}} \frac{\partial \tilde{u}_0}{\partial \mathbf{n}_F} \, \mathrm{d}s = 0,$$

$$\text{and} \quad \int_{\tilde{F}_{\mathrm{p}} \setminus F_{\mathrm{p}}} f \, \mathrm{d}x + \int_{\tilde{\gamma}} \tilde{g} \, \mathrm{d}s - \int_{\gamma_{\mathrm{r}}} \frac{\partial \tilde{u}_0}{\partial \mathbf{n}_F} \, \mathrm{d}s = 0.$$

Consequently,

$$\overline{d_{\gamma_{0,\mathrm{p}}}}^{\gamma_{0,\mathrm{p}}} = \overline{\left(g_0 + \frac{\partial \tilde{u}_0}{\partial \mathbf{n}_F} \right)}^{\gamma_{0,\mathrm{p}}} = \frac{1}{|\gamma_{0,\mathrm{p}}|} \left(\int_{\gamma_{0,\mathrm{p}}} g_0 \, \mathrm{d}s - \int_{\gamma_{\mathrm{p}}} g \, \mathrm{d}s - \int_{F_{\mathrm{p}}} f \, \mathrm{d}x \right),$$

$$\overline{d_{\gamma_{\mathrm{r}}}}^{\gamma_{\mathrm{r}}} = \overline{\left(g - \frac{\partial \tilde{u}_0}{\partial \mathbf{n}_F} \right)}^{\gamma_{\mathrm{r}}} = \frac{1}{|\gamma_{\mathrm{r}}|} \left(\int_{\gamma_{\mathrm{r}}} g \, \mathrm{d}s - \int_{\tilde{\gamma}} \tilde{g} \, \mathrm{d}s - \int_{\tilde{F}_{\mathrm{p}} \setminus F_{\mathrm{p}}} f \, \mathrm{d}x \right).$$

Moreover, as in Remark 4.1, it can be seen that

$$\overline{d_{\gamma_{\mathrm{n}}}}^{\gamma_{\mathrm{n}}} = \frac{1}{|\gamma_{\mathrm{n}}|} \left(\int_{\gamma_{\mathrm{n}}} g \, \mathrm{d}s - \int_{\gamma_{0,\mathrm{n}}} g_0 \, \mathrm{d}s - \int_{F_{\mathrm{n}}} f \, \mathrm{d}x \right).$$

Therefore, the terms involving the average values of d_σ in the estimator $\mathcal{E}(u_{\mathrm{d}})$ defined in (24) only depend on the defeatured problem data. More precisely, they only depend on the choice of g_0 and $\tilde{g}$ that one chooses on γ_0 and $\tilde{\gamma}$ respectively, and on the choice of the extension of f that one considers in the extended feature $\tilde{F}_{\mathrm{p}}$. As a consequence, if those terms dominate, this means that the defeatured problem data should be better chosen. Moreover, under the following reasonable flux conservation assumptions

$$\int_{\gamma_{0,\mathrm{p}}} g_0 \, \mathrm{d}s = \int_{\gamma_{\mathrm{p}}} g \, \mathrm{d}s + \int_{F_{\mathrm{p}}} f \, \mathrm{d}x, \qquad \int_{\tilde{\gamma}} \tilde{g} \, \mathrm{d}s = \int_{\gamma_{\mathrm{r}}} g \, \mathrm{d}s - \int_{\tilde{F}_{\mathrm{p}} \setminus F_{\mathrm{p}}} f \, \mathrm{d}x,$$

$$\text{and} \quad \int_{\gamma_{0,\mathrm{n}}} g_0 \, \mathrm{d}s = \int_{\gamma_{\mathrm{n}}} g \, \mathrm{d}s - \int_{F_{\mathrm{n}}} f \, \mathrm{d}x, \tag{25}$$

the defeaturing error estimator (24) rewrites $\mathcal{E}(u_{\mathrm{d}}) := \left(\sum_{\sigma \in \Sigma} |\sigma|^{\frac{1}{n-1}} \|d_\sigma\|_{0,\sigma}^2 \right)^{\frac{1}{2}}$. Conditions (25) are easily met if the Neumann boundary condition g and the source function f are zero in the vicinity of the feature.

Remark 5.4 Analogously to the case of a negative feature in Remark 4.2, note that

$$\mathcal{E}(u_{\mathrm{d}}) \lesssim \left(\sum_{\sigma \in \Sigma} c_\sigma^2 |\sigma|^{\frac{1}{n-1}} \|d_\sigma\|_{0,\sigma}^2 \right)^{\frac{1}{2}} =: \tilde{\mathcal{E}}(u_{\mathrm{d}}).$$

One could be tempted to use the simpler indicator $\tilde{\mathcal{E}}(u_{\mathrm{d}})$, but when $n = 2$ and under the flux conservation conditions (25), $\tilde{\mathcal{E}}(u_{\mathrm{d}})$ is sub-optimal since in this case, $\tilde{\mathcal{E}}(u_{\mathrm{d}}) \lesssim \max_{\sigma \in \Sigma}(c_\sigma) \mathcal{E}(u_{\mathrm{d}})$. Indeed, no lower bound can be proven for $\tilde{\mathcal{E}}(u_{\mathrm{d}})$.

5.2.1 Upper bound

In this section, we prove that the error indicator defined in (24) is reliable, that is, it is an upper bound for the defeaturing error.

Theorem 5.5 *Let u_{d} be the defeaturing solution as defined in (22). If γ_{n}, γ_{r} and $\gamma_{0,\mathrm{p}}$ are isotropic according to Definition 2.1, then the defeaturing error in energy norm is bounded in terms of the estimator $\mathcal{E}(u_{\mathrm{d}})$ introduced in (24) as follows:*

$$|u - u_{\mathrm{d}}|_{1,\Omega} \lesssim \mathcal{E}(u_{\mathrm{d}}).$$

Proof. Using arguments similar to Theorem 4.3, let us first consider the original problem (1) restricted to $\Omega^{\star} := \Omega \setminus \overline{F_{\mathrm{p}}}$ with the natural Neumann boundary condition on $\gamma_{0,\mathrm{p}}$, that is the restriction $u|_{\Omega^{\star}} \in H^1_{h,\Gamma_D}(\Omega^{\star})$ is the weak solution of

$$\begin{cases} -\Delta \left(u|_{\Omega^{\star}} \right) = f & \text{in } \Omega^{\star} \\ u|_{\Omega^{\star}} = h & \text{on } \Gamma_D \\ \dfrac{\partial \left(u|_{\Omega^{\star}} \right)}{\partial \mathbf{n}} = g & \text{on } \Gamma_N \setminus \gamma_{\mathrm{p}} \\ \dfrac{\partial \left(u|_{\Omega^{\star}} \right)}{\partial \mathbf{n_0}} = \dfrac{\partial u}{\partial \mathbf{n_0}} & \text{on } \gamma_{0,\mathrm{p}}. \end{cases} \tag{26}$$

By abuse of notation, we omit the explicit restriction of u to $\Omega^{\star}$. Then for all $v_0 \in H^1_{0,\Gamma_D}(\Omega^{\star})$,

$$\int_{\Omega^{\star}} \nabla u \cdot \nabla v_0 \, \mathrm{d}x = \int_{\Omega^{\star}} f v_0 \, \mathrm{d}x + \int_{\Gamma_N \setminus \gamma_{\mathrm{p}}} g v_0 \, \mathrm{d}s + \int_{\gamma_{0,\mathrm{p}}} \frac{\partial u}{\partial \mathbf{n_0}} v_0 \, \mathrm{d}s. \tag{27}$$

Then, let us consider the simplified problem (3) restricted to $\Omega^{\star}$ with the natural Neumann boundary condition on γ_{n}, in the same way as in (11). Thus, since by definition $u_{\mathrm{d}}|_{\Omega^{\star}} = u_0|_{\Omega^{\star}}$, and if we omit the explicit restriction of u_{d} to $\Omega^{\star}$, for all $v_0 \in H^1_{0,\Gamma_D}(\Omega^{\star})$,

$$\int_{\Omega^{\star}} \nabla u_{\mathrm{d}} \cdot \nabla v_0 \, \mathrm{d}x = \int_{\Omega^{\star}} f v_0 \, \mathrm{d}x + \int_{\Gamma_N \setminus \gamma} g v_0 \, \mathrm{d}s + \int_{\gamma_{\mathrm{n}}} \frac{\partial u_{\mathrm{d}}}{\partial \mathbf{n}} v_0 \, \mathrm{d}s + \int_{\gamma_{0,\mathrm{p}}} g_0 v_0 \, \mathrm{d}s. \tag{28}$$

Let $e := u - u_{\mathrm{d}} \in H^1_{0,\Gamma_D}(\Omega)$. So from (27) and (28), for all $v_0 \in H^1_{0,\Gamma_D}(\Omega^{\star})$, we obtain

$$\int_{\Omega^{\star}} \nabla e \cdot \nabla v_0 \, \mathrm{d}x = \int_{\gamma_{\mathrm{n}}} \left(g - \frac{\partial u_{\mathrm{d}}}{\partial \mathbf{n}} \right) v_0 \, \mathrm{d}s + \int_{\gamma_{0,\mathrm{p}}} \left(\frac{\partial u}{\partial \mathbf{n_0}} - g_0 \right) v_0 \, \mathrm{d}s. \tag{29}$$

Now, let us consider the simplified extended problem (6) restricted to F_{p} with the natural Neumann boundary condition on γ_{r}, in a similar way to (26). Note that $u_{\mathrm{d}}|_{F_{\mathrm{p}}} = \tilde{u}_0|_{F_{\mathrm{p}}}$, and by abuse of notation and as previously, we omit the explicit restriction of u_{d} to F_{p}. That is, $u_{\mathrm{d}} \in H^1(F_{\mathrm{p}})$ is one of the infinitely-many solutions (up to a constant) of

$$\int_{F_{\mathrm{p}}} \nabla u_{\mathrm{d}} \cdot \nabla v_{\mathrm{p}} \, \mathrm{d}x = \int_{F_{\mathrm{p}}} f v_{\mathrm{p}} \, \mathrm{d}x + \int_{\gamma_{\mathrm{s}}} g v_{\mathrm{p}} \, \mathrm{d}s + \int_{\gamma_{0,\mathrm{p}} \cup \gamma_{\mathrm{r}}} \frac{\partial u_{\mathrm{d}}}{\partial \mathbf{n}_F} v_{\mathrm{p}} \, \mathrm{d}s, \qquad \forall v_{\mathrm{p}} \in H^1(F_{\mathrm{p}}). \tag{30}$$

And let us consider the original problem (1) restricted to F_{p} with the natural Neumann boundary condition on $\gamma_{0,\mathrm{p}}$, again in a similar way to (26). By abuse of notation and as previously, we omit the explicit restriction of u to F_{p}. So $u \in H^1(F_{\mathrm{p}})$ is one of the infinitely-many solutions (up to a constant) of

$$\int_{F_{\mathrm{p}}} \nabla u \cdot \nabla v_{\mathrm{p}} \, \mathrm{d}x = \int_{F_{\mathrm{p}}} f v_{\mathrm{p}} \, \mathrm{d}x + \int_{\gamma_{\mathrm{p}}} g v_{\mathrm{p}} \, \mathrm{d}x + \int_{\gamma_{0,\mathrm{p}}} \frac{\partial u}{\partial \mathbf{n}_F} v_{\mathrm{p}} \, \mathrm{d}s, \qquad \forall v_{\mathrm{p}} \in H^1(F_{\mathrm{p}}). \tag{31}$$

Consequently, from (30) and (31), for all $v_{\mathrm{p}} \in H^1(F_{\mathrm{p}})$,

$$\int_{F_{\mathrm{p}}} \nabla e \cdot \nabla v_{\mathrm{p}} \, \mathrm{d}x = \int_{\gamma_{0,\mathrm{p}}} \frac{\partial (u - u_{\mathrm{d}})}{\partial \mathbf{n}_F} v_{\mathrm{p}} \, \mathrm{d}s + \int_{\gamma_{\mathrm{r}}} \left(g - \frac{\partial u_{\mathrm{d}}}{\partial \mathbf{n}} \right) v_{\mathrm{p}} \, \mathrm{d}s. \tag{32}$$

Let $v \in H^1_{0,\Gamma_D}(\Omega)$, then $v|_{\Omega^\star} \in H^1_{0,\Gamma_D}(\Omega^\star)$ and $v|_{F_p} \in H^1(F_p)$. Therefore, from equations (29) and (32), since $\mathbf{n}_0 = -\mathbf{n}_F$ on $\gamma_{0,p}$ and recalling the definitions of Σ and d_σ in (23), we obtain

$$\int_\Omega \nabla e \cdot \nabla v \, \mathrm{d}x = \sum_{\sigma \in \Sigma} \int_\sigma d_\sigma v \, \mathrm{d}s. \tag{33}$$

Now, if we take $v = e \in H^1_{0,\Gamma_D}(\Omega)$ in (33), then

$$|e|^2_{1,\Omega} = \sum_{\sigma \in \Sigma} \int_\sigma d_\sigma e \, \mathrm{d}s = \sum_{\sigma \in \Sigma} \left[\int_\sigma \left(d_\sigma - \overline{d_\sigma}^\sigma \right) (e - \overline{e}^\sigma) \, \mathrm{d}s + \overline{d_\sigma}^\sigma \int_\sigma e \, \mathrm{d}s \right]. \tag{34}$$

For each $\sigma \in \Sigma$, the first terms of (34) can be estimated as in (15), using Appendix A.1, trace inequalities and the discrete Cauchy-Schwarz inequality. Thus we obtain

$$\sum_{\sigma \in \Sigma} \int_\sigma \left(d_\sigma - \overline{d_\sigma}^\sigma \right) (e - \overline{e}^\sigma) \, \mathrm{d}s \lesssim \sum_{\sigma \in \Sigma} |\sigma|^{\frac{1}{2(n-1)}} \left\| d_\sigma - \overline{d_\sigma}^\sigma \right\|_{0,\sigma} |e|_{\frac{1}{2},\sigma}$$

$$\lesssim |\gamma_n|^{\frac{1}{2(n-1)}} \left\| d_{\gamma_n} - \overline{d_{\gamma_n}}^{\gamma_n} \right\|_{0,\gamma_n} \|e\|_{1,\Omega^\star}$$

$$+ \left(\sum_{\sigma \in \{\gamma_{0,p}, \gamma_r\}} |\sigma|^{\frac{1}{2(n-1)}} \left\| d_\sigma - \overline{d_\sigma}^\sigma \right\|_{0,\sigma} \right) \|e\|_{1,F_p}$$

$$\lesssim \left(\sum_{\sigma \in \Sigma} |\sigma|^{\frac{1}{n-1}} \left\| d_\sigma - \overline{d_\sigma}^\sigma \right\|^2_{0,\sigma} \right)^{\frac{1}{2}} |e|_{1,\Omega}. \tag{35}$$

Moreover, for each $\sigma \in \Sigma$, the last terms of (34) can be estimated using Appendix A.2, trace inequalities and the discrete Cauchy-Schwarz inequality to obtain

$$\sum_{\sigma \in \Sigma} \overline{d_\sigma}^\sigma \int_\sigma e \, \mathrm{d}s \lesssim \sum_{\sigma \in \Sigma} \left| \overline{d_\sigma}^\sigma \right| |\sigma|^{\frac{1}{2}} \|e\|_{0,\sigma}$$

$$\lesssim \left(\sum_{\sigma \in \{\gamma_n, \gamma_{0,p}\}} \left| \overline{d_\sigma}^\sigma \right| c_\sigma |\sigma|^{\frac{1}{2(n-1)} + \frac{1}{2}} \right) \|e\|_{\frac{1}{2},\partial\Omega^\star}$$

$$+ \left| \overline{d_{\gamma_r}}^{\gamma_r} \right| c_{\gamma_r} |\gamma_r|^{\frac{1}{2(n-1)} + \frac{1}{2}} \|e\|_{\frac{1}{2},\partial\Omega}$$

$$\lesssim \left(\sum_{\sigma \in \Sigma} c^2_\sigma |\gamma_\sigma|^{\frac{n}{n-1}} \left| \overline{d_\sigma}^\sigma \right|^2 \right)^{\frac{1}{2}} |e|_{1,\Omega}. \tag{36}$$

Therefore, combining (34), (35) and (36), and simplifying on both sides, we obtain the desired result. $\qquad \square$

5.2.2 Lower bound

In this section, we prove that the error indicator defined in (24) is efficient, that is, it is a lower bound for the defeaturing error, up to oscillations. In the case $n = 2$, the flux conservation assumptions (25) are also required.

Theorem 5.6 *Consider the same notation and assumptions as in Theorem 5.5, and assume that all $\sigma \in \Sigma$ are also regular according to Definition 2.2 with $|\gamma_n| \simeq |\gamma_r| \simeq |\gamma_{0,p}|$. Suppose that either $n = 3$, or $n = 2$ and the flux conservation conditions (25) are satisfied. Then the defeaturing error, in energy norm, bounds up to oscillations the estimator $\mathcal{E}(u_d)$ introduced in (24), that is*

$$\mathcal{E}(u_d) \lesssim |u - u_d|_{1,\Omega} + \mathrm{osc}(u_d),$$

where

$$\text{osc}(u_{\text{d}}) := |\Gamma|^{\frac{1}{2(n-1)}} \left(\sum_{\sigma \in \Sigma} \|d_\sigma - \Pi_m(d_\sigma)\|_{0,\sigma}^2 \right)^{\frac{1}{2}} \tag{37}$$

for any $m \in \mathbb{N}$, with $\Gamma := \gamma_{\text{n}} \cup \gamma_{\text{r}} \cup \gamma_{0,\text{p}}$, Σ and d_σ defined as in (23) and Π_m such that $\Pi_m|_\sigma \equiv \Pi_{m,\sigma}$ for all $\sigma \in \Sigma$, $\Pi_{m,\sigma}$ being extensions of the Clément operator as defined in Sec. 2.

Proof. As before, let $e := u - u_{\text{d}} \in H^1_{0,\Gamma_D}(\Omega)$. Then from equation (33), for all $v \in H^1_{0,\Gamma_D}(\Omega)$,

$$\sum_{\sigma \in \Sigma} \int_\sigma d_\sigma v \, \text{d}s = \int_\Omega \nabla e \cdot \nabla v \, \text{d}x \le |e|_{1,\Omega} |v|_{1,\Omega}. \tag{38}$$

Now, let $H := \left\{ v \in H^{\frac{1}{2}}_{00}(\Gamma) : v|_\sigma \in H^{\frac{1}{2}}_{00}(\sigma), \text{ for all } \sigma \in \Sigma \right\}$, equipped with the norm

$$\|\cdot\|_H := \left(\sum_{\sigma \in \Sigma} \|\cdot\|_{H^{1/2}_{00}(\sigma)}^2 \right)^{\frac{1}{2}},$$

and let H^* be its dual space equipped with the dual norm $\|\cdot\|_{H^*}$. Recall that $\Omega^\star := \Omega \setminus \overline{F_{\text{p}}}$, so that $\Omega = \text{int}\left(\overline{\Omega^\star} \cup \overline{F_{\text{p}}}\right)$. So for all $w \in H$, let us define piecewise the function $u_w \in H^1_{0,\partial\Omega\setminus(\gamma_{\text{n}}\cup\gamma_{\text{r}})}(\Omega)$ as the unique solution of

$$\begin{cases} -\Delta\left(u_w|_{F_{\text{p}}}\right) = 0 & \text{in } F_{\text{p}} \\ u_w|_{F_{\text{p}}} = \left(w|_{\gamma_{\text{r}}\cup\gamma_{0,\text{p}}}\right)^\star & \text{on } \partial F_{\text{p}}, \end{cases} \qquad \begin{cases} -\Delta\left(u_w|_{\Omega^\star}\right) = 0 & \text{in } \Omega^\star \\ u_w|_{\Omega^\star} = \left(w|_{\gamma_{\text{n}}\cup\gamma_{0,\text{p}}}\right)^\star & \text{on } \partial\Omega^\star, \end{cases}$$

where $\left(w|_{\gamma_{\text{r}}\cup\gamma_{0,\text{p}}}\right)^\star$ and $\left(w|_{\gamma_{\text{n}}\cup\gamma_{0,\text{p}}}\right)^\star$ are the extensions by 0 of $w|_{\gamma_{\text{r}}\cup\gamma_{0,\text{p}}}$ on ∂F_{p} and of $w|_{\gamma_{\text{n}}\cup\gamma_{0,\text{p}}}$ on $\partial\Omega^\star$, respectively. Then by continuity of the solution on the data and from Appendix A.6,

$$\begin{aligned}
|u_w|_{1,\Omega} &= \left(|u_w|_{1,F_{\text{p}}}^2 + |u_w|_{1,\Omega^\star}^2 \right)^{\frac{1}{2}} \\
&\lesssim \left(\left\| \left(w|_{\gamma_{\text{r}}\cup\gamma_{0,\text{p}}}\right)^\star \right\|_{\frac{1}{2},\partial F_{\text{p}}}^2 + \left\| \left(w|_{\gamma_{\text{n}}\cup\gamma_{0,\text{p}}}\right)^\star \right\|_{\frac{1}{2},\partial\Omega^\star}^2 \right)^{\frac{1}{2}} \\
&= \left(\|w\|_{H^{1/2}_{00}(\gamma_{\text{r}}\cup\gamma_{0,\text{p}})}^2 + \|w\|_{H^{1/2}_{00}(\gamma_{\text{n}}\cup\gamma_{0,\text{p}})}^2 \right)^{\frac{1}{2}} \lesssim \|w\|_H.
\end{aligned} \tag{39}$$

So, recalling that by definition, $d_\Sigma|_\sigma = d_\sigma$ on each $\sigma \in \Sigma$, thanks to (38) and (39) and since $H^1_{0,\partial\Omega\setminus(\gamma_{\text{n}}\cup\gamma_{\text{r}})}(\Omega) \subset H^1_{0,\Gamma_D}(\Omega)$, then

$$\begin{aligned}
\|d_\Sigma\|_{H^*} = \sup_{\substack{w \in H \\ w \ne 0}} \frac{\int_\Gamma d_\Sigma w \, \text{d}s}{\|w\|_H} &\lesssim \sup_{\substack{w \in H \\ w \ne 0}} \frac{\sum_{\sigma \in \Sigma} \int_\sigma d_\sigma u_w \, \text{d}s}{|u_w|_{1,\Omega}} \\
&\le \sup_{\substack{v \in H^1_{0,\Gamma_D}(\Omega) \\ v \ne 0}} \frac{\sum_{\sigma \in \Sigma} \int_\sigma d_\sigma v \, \text{d}s}{|v|_{1,\Omega}} \le |e|_{1,\Omega}.
\end{aligned} \tag{40}$$

Moreover, using Remark 5.4 if $n = 3$, or Remark 5.3 if $n = 2$ and if the flux conservation conditions (25) are satisfied, then

$$\mathcal{E}(u_{\text{d}}) \lesssim \left(\sum_{\sigma \in \Sigma} |\sigma|^{\frac{1}{n-1}} \|d_\sigma\|_{0,\sigma}^2 \right)^{\frac{1}{2}}.$$

Therefore, using the triangle inequality, and the fact that $|\gamma_n| \simeq |\gamma_r| \simeq |\gamma_{0,p}| \simeq |\Gamma|$, then

$$\mathcal{E}(u_d)^2 \leq \sum_{\sigma \in \Sigma} |\sigma|^{\frac{1}{n-1}} \|\Pi_m(d_\sigma)\|_{0,\sigma}^2 + \sum_{\sigma \in \Sigma} \|d_\sigma - \Pi_m(d_\sigma)\|_{0,\sigma}^2$$

$$\lesssim |\Gamma|^{\frac{1}{n-1}} \|\Pi_m(d_\Sigma)\|_{0,\Gamma}^2 + |\Gamma|^{\frac{1}{n-1}} \|d_\Sigma - \Pi_m(d_\Sigma)\|_{0,\Gamma}^2.$$

Now, we use the definition of the broken norm in H^* to apply the inverse inequality of Appendix A.7. Recalling the definition (37) of the oscillations, and using again the triangle inequality, we thus obtain

$$\mathcal{E}(u_d)^2 \lesssim \|\Pi_m(d_\Sigma)\|_{H^*}^2 + \operatorname{osc}(u_d)^2$$

$$\lesssim \left[\|d_\Sigma\|_{H^*} + \|\Pi_m(d_\Sigma) - d_\Sigma\|_{H^*} + \operatorname{osc}(u_d) \right]^2. \tag{41}$$

Furthermore, applying Appendix A.6 and then Appendix A.4, we have

$$\|\Pi_m(d_\Sigma) - d_\Sigma\|_{H^*} \lesssim \|\Pi_m(d_\Sigma) - d_\Sigma\|_{H_{00}^{-1/2}(\Gamma)}$$

$$\lesssim |\Gamma|^{\frac{1}{2(n-1)}} \|\Pi_m(d_\Sigma) - d_\Sigma\|_{0,\Gamma} = \operatorname{osc}(u_d). \tag{42}$$

To conclude, we plug in (40) and (42) into equation (41), and thus

$$\mathcal{E}(u_d) \lesssim |e|_{1,\Omega} + \operatorname{osc}(u_d).$$

$\square$

Remark 5.7 As in Remark 4.5, when the data is regular, it is always possible to choose m large enough so that the asymptotic behavior of the oscillations is $\mathcal{O}\left(|\Gamma|^{m + \frac{1}{2(n-1)}}\right)$. Therefore, we can make sure that the oscillations get small with respect to the defeaturing error, when the feature gets small.

6 Numerical considerations and experiments

From the definition of the *a posteriori* defeaturing error estimator (24) in the general case, to estimate the error introduced by defeaturing the problem geometry, we only need to perform the following steps.

(i) Choose the Neumann data g_0 and solve the defeatured problem (3).

(ii) For the positive component F_p of the feature F, choose the Neumann data $\tilde{g}$ and solve the local extension problem (5). However, features may be geometrically complex, and the solution of the extension problem an unwanted burden. Therefore, instead of (5), one can solve the extension problem (6) in a chosen (simple) domain $\tilde{F}_p$ that contains F_p and such that $\gamma_{0,p} \subset \left(\partial\tilde{F}_p \cap \partial F_p\right)$.

(iii) Compute the boundary averages and integrals $\overline{d_\sigma}^\sigma$ and $\left\|d_\sigma - \overline{d_\sigma}^\sigma\right\|_{0,\sigma}$ for each $\sigma \in \Sigma$, as defined in (23). That is, we suitably evaluate the error made on the normal derivative of the solution on specific parts of the boundaries of the features.

In the remaining part of the paper, we present a few numerical examples to illustrate the validity of our defeaturing error estimator. All the numerical experiments presented in the following section have been implemented in GeoPDEs [47], an open-source and free Octave/Matlab package for the resolution of partial differential equations specifically designed for isogeometric analysis [3]. For the geometric description of the features and the local meshing process required, multipatch and trimming techniques have been used [13, 48]. Moreover, a rather fine mesh is used in order to neglect the error due to the numerical approximation.
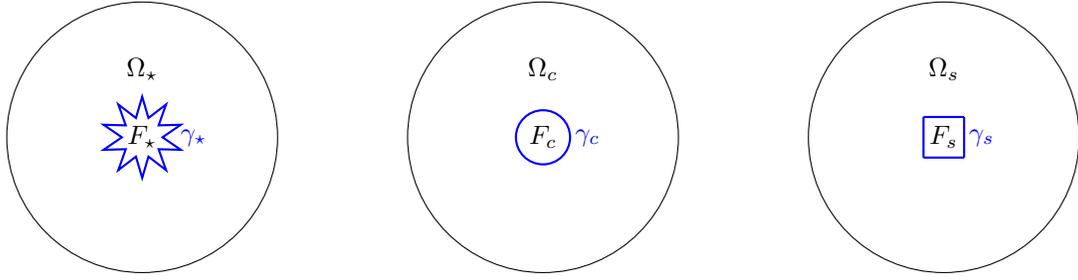
(a) Domain with a star feature.   (b) Domain with a circle feature.   (c) Domain with a square feature.

Figure 6: Comparison between feature shapes.

Domain Ω	Perimeter of F	Area of F	$\mathcal{E}(u_0)$	$|u - u_0|_{1,\Omega}$	$\dfrac{|u - u_0|_{1,\Omega}}{|u_0|_{0,\Omega}}$	Eff. index
$\Omega_\star,\ r_\star = 1.83 \cdot 10^{-2}$	0.400	$2.07 \cdot 10^{-3}$	$1.98 \cdot 10^{-3}$	$1.56 \cdot 10^{-3}$	$2.49 \cdot 10^{-3}$	1.27
$\Omega_c,\ r_c = 6.37 \cdot 10^{-2}$	0.400	$1.27 \cdot 10^{-2}$	$1.21 \cdot 10^{-2}$	$8.42 \cdot 10^{-3}$	$1.34 \cdot 10^{-2}$	1.45
$\Omega_s,\ r_s = 5.00 \cdot 10^{-2}$	0.400	$1.00 \cdot 10^{-2}$	$9.57 \cdot 10^{-3}$	$6.74 \cdot 10^{-3}$	$1.07 \cdot 10^{-2}$	1.42
$\Omega_c,\ r_c = 5.64 \cdot 10^{-2}$	0.355	$1.00 \cdot 10^{-2}$	$1.01 \cdot 10^{-2}$	$6.76 \cdot 10^{-3}$	$1.08 \cdot 10^{-2}$	1.51
$\Omega_\star,\ r_\star = 4.02 \cdot 10^{-2}$	0.880	$1.00 \cdot 10^{-2}$	$7.53 \cdot 10^{-3}$	$6.65 \cdot 10^{-3}$	$1.38 \cdot 10^{-2}$	1.13

Table 1: Results of the comparison between feature shapes.

6.1 Impact of some properties of the feature on the defeaturing error

While validating the theory developed in Sec. 4 and Sec. 5, we study the impact of the shape and the size of a feature on the defeaturing error and estimator, and of the choice of the defeatured Neumann data. Moreover, as the estimator depends upon the size of the features and the size of the solution gradients "around" the feature, we will be able to show an example where small features count more than big ones.

6.1.1 Feature shape

In this example, we compare the behavior of the error and the estimator on the same Poisson problem in three different geometries: one with a star-shaped feature, another one with a circular feature, and the last one with a squared feature. Let

$$\Omega_0 := \left\{ \big(r\cos(\theta), r\sin(\theta) \big) \in \mathbb{R}^2 : 0 \leq r < 1, 0 \leq \theta \leq 2\pi \right\},$$

let $\Omega_\star := \Omega_0 \setminus \overline{F_\star}$, $\Omega_c := \Omega_0 \setminus \overline{F_c}$ and $\Omega_s := \Omega_0 \setminus \overline{F_s}$, with

- $F_\star$ the 10-branch regular star of inner radius $r_\star > 0$, outer radius $2r_\star$, centered in $(0,0)$,

- F_c the circle of radius $r_c > 0$, centered in $(0,0)$,

- F_s the square of side length $2r_s > 0$, centered in $(0,0)$,

as in Fig. 6.

We choose $r_\star, r_c, r_s > 0$ such that $F_\star$, F_c and F_s have, first, the same area, and then, the same perimeter. We consider Poisson problem (1) solved in $\Omega_\star$, Ω_c and in Ω_s, and its defeatured version (3). We take $f \equiv 1$ in Ω_0, $h \equiv 0$ on $\Gamma_D := \partial\Omega_0$, and $g \equiv 0$ on $\partial F_\star$, on ∂F_c and on ∂F_s.

The results are summarized in Table 1. We can see that in all the cases, the larger the area of the feature, the larger the defeaturing error and estimator. Moreover, the effectivity index only changes slightly
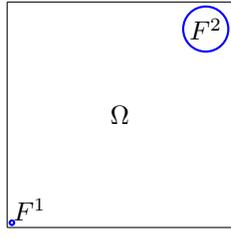
(a) Exact domain Ω with two features (not at scale).
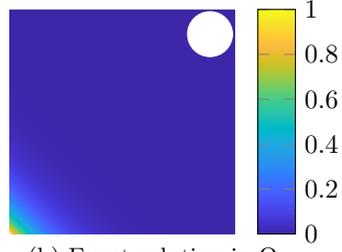
(b) Exact solution in Ω.

Figure 7: Geometry with two features of different size and exact solution.

$\mathcal{E}^1(u_0)$	$\mathcal{E}^2(u_0)$	$\mathcal{E}(u_0)$	$\big|u - u_0\big|_{1,\Omega}$	$\dfrac{\big|u - u_0\big|_{1,\Omega}}{\big|u_0\big|_{0,\Omega}}$	Effectivity index
$5.03 \cdot 10^{-2}$	$7.86 \cdot 10^{-6}$	$5.03 \cdot 10^{-2}$	$1.45 \cdot 10^{-2}$	$2.05 \cdot 10^{-2}$	3.47

Table 2: Results of the comparison between feature sizes.

when considering the same feature but with different measures: this shows that it is indeed independent from the measure of the considered feature and its boundary. The small change in the effectivity index is only due to numerical approximation, the solutions not being exact but being obtained on a very fine mesh. Furthermore, the shape of the feature does not impact much the defeaturing estimator: we do not observe any major difference between the smooth feature (the circle), the convex non-smooth Lipschitz feature (the square), and the non-convex non-smooth Lipschitz feature (the star). Our theory indeed treats those different types of geometries in the same way. Finally, even if the estimator is referred to the absolute error, both the relative and the absolute errors are given to be able to quantify the magnitude of the defeaturing effect.

6.1.2 Feature size

Removing a small feature where the solution of the PDE has a high gradient can significantly increase the defeaturing error, while the error might almost not be affected when removing a large feature where the solution of the PDE is nearly constant. The following example shows that our estimator is also able to capture this. Let $\Omega_0 := (0,1)^2$ and $\Omega := \Omega_0 \setminus \left(\overline{F^1} \cup \overline{F^2} \right)$, where F^1 and F^2 are circles of two different sizes given by

$$F^1 := \big\{ (1.1 \cdot 10^{-3}, 1.1 \cdot 10^{-3}) + \big(r\cos(\theta), r\sin(\theta) \big) \in \mathbb{R}^2 :$$
$$0 \le r < 10^{-3}, 0 \le \theta \le 2\pi \big\},$$
$$F^2 := \big\{ (8.9 \cdot 10^{-1}, 8.9 \cdot 10^{-1}) + \big(r\cos(\theta), r\sin(\theta) \big) \in \mathbb{R}^2 :$$
$$0 \le r < 10^{-1}, 0 \le \theta \le 2\pi \big\},$$

similarly as in Fig. 7a. We consider Poisson problem (1) solved in Ω, and its defeatured version (3) in Ω_0. Let $f(x,y) := -128e^{-8(x+y)}$ in Ω_0, $h(x,y) := e^{-8(x+y)}$ on

$$\Gamma_D := \big\{ (x,0), (0,y) \in \mathbb{R}^2 : 0 \le x, y < 1 \big\},$$

the bottom and left sides, $g(x,y) := -8e^{-8(x+y)}$ on $\partial\Omega_0 \setminus \overline{\Gamma_D}$, and finally $g \equiv 0$ on $\partial F^1 \cup \partial F^2$. Since the geometry contains two features, we call $\mathcal{E}^1$ and $\mathcal{E}^2$ the defeaturing estimators defined in (8) and computed, respectively, on the boundary of F^1 and on the boundary of F^2, and we consider the sum of $\mathcal{E}^1$ and $\mathcal{E}^2$ as the total defeaturing estimator $\mathcal{E}$.

With this choice, the solution to Poisson problem has a very high gradient near feature F^1, and it is almost constantly zero near feature F^2, as we can observe in Fig. 7b. Therefore, one can expect the presence

(a) Geometry with the negative feature F_ε^1.

(b) Geometry with the negative feature F_ε^2.

(c) Geometry with the positive feature F_ε^3.

(d) Geometry with the positive feature F_ε^4.
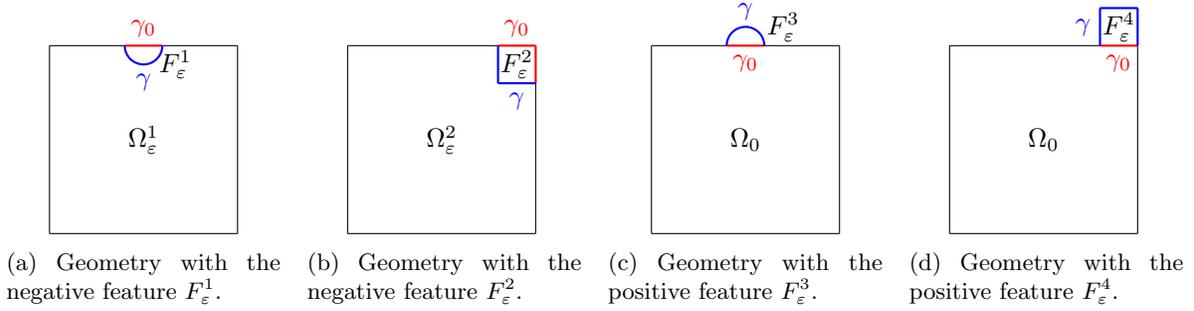
Figure 8: 2D geometries Ω_ε^i, $i = 1, 2, 3, 4$.

of F^1 to be more important than F^2 with respect to the solution accuracy, even if F^1 is notably smaller than F^2. The results are presented in Table 2, where we can see that this is indeed the case: the estimator on F^2 is four orders of magnitude smaller than the estimator on F^1, even if the radius of F^1 is two orders of magnitude smaller than the one of F^2. This confirms the fact that our estimator as written in (24) correctly trades off the measure of the features and their position in the geometrical domain, in order to correctly assess the impact of defeaturing on the solution.

Finally, and as in the previous numerical experiment of Sec. 6.1.2, both the relative error and the absolute error are given to be able to quantify the magnitude of the defeaturing effect. In the following, we will be interested in the convergence of the error and estimator with respect to the size of the feature. Since the relative error is a scaling of the absolute error, the convergence will be the same whether one considers the relative or the absolute error. Moreover, since the magnitude of the error depends on the problem at hand (geometries, size of the feature, and PDE data), and since the derived estimator is referred to the absolute error, we will only look at the absolute defeaturing error in the next experiments.

6.2 Error convergence with respect to the feature size

We now analyze the convergence of our estimator with respect to the size of the feature and we compare it with the convergence of the defeaturing error. Moreover, we show an example in which the choice of the defeatured problem data influences drastically the convergence of both the estimator and the defeaturing error.

6.2.1 Two-dimensional geometries

We begin with two-dimensional examples of geometries with a negative feature. For $k = 0, 1, \ldots, 6$, let $\varepsilon = \dfrac{10^{-2}}{2^k}$, and let $\Omega_\varepsilon^i := \Omega_0 \setminus \overline{F_\varepsilon^i}$ for $i = 1, 2$ with $\Omega_0 := (0, 1)^2$ and

$$F_\varepsilon^1 := \left\{ \left(0.5 + r\cos(\theta), 1 + r\sin(\theta)\right) \in \mathbb{R}^2 : 0 \leq r < \varepsilon, -\pi < \theta < 0 \right\},$$
$$F_\varepsilon^2 := (1 - \varepsilon, 1)^2,$$

as in Fig. 8a and Fig. 8b. For $i = 1, 2$, we consider Poisson problem (1) solved in Ω_ε^i, and its defeatured version (3) in Ω_0. We take $f(x, y) := 10\cos(3\pi x)\sin(5\pi y)$ in Ω_0, $h \equiv 0$ on

$$\Gamma_D := \left\{ (x, 0) \in \mathbb{R}^2 : 0 < x < 1 \right\},$$

$g \equiv 0$ on $\Gamma_N := \partial\Omega_\varepsilon^i \setminus \overline{\Gamma_D}$, and $g_0 \equiv 0$ on $\partial\Omega_0 \setminus \partial\Omega_\varepsilon^i$. We respectively call $u^{(i)}$ and $u_0^{(i)}$ the exact and defeatured solutions.

The results are presented in Fig. 9a. Both the error and the estimator converge with respect to the size of the feature as $\varepsilon \propto |\gamma|$ in the first geometry Ω_ε^1, and as $\varepsilon^2 \propto |\gamma|^2$ in the second geometry Ω_ε^2. Clearly,

(a) Geometries Ω_ε^1 and Ω_ε^2 with a negative feature.

(b) Geometries Ω_ε^3 and Ω_ε^4 with a positive feature.

(c) Geometry Ω_ε^5 with a general complex feature.

(d) Geometry Ω_ε^6 with a general complex feature.
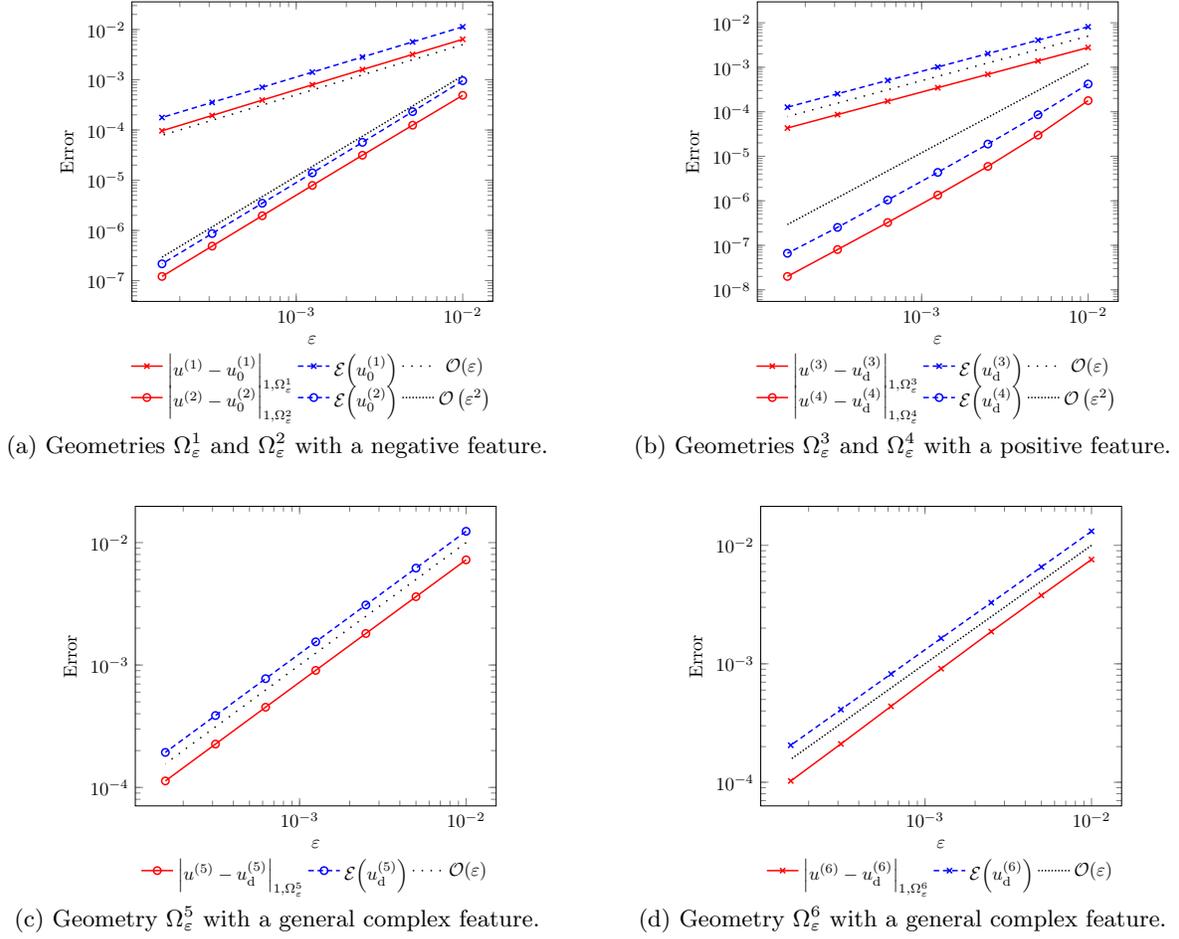
Figure 9: Convergence of the error and of the estimator in 2D domains with one feature.

the difference in asymptotic behavior of the error depends on symmetries and on the Neumann boundary conditions. Indeed, Ω_ε^2 has features with sides parallel to $\partial\Omega_0$. Moreover, the effectivity index is indeed independent from the size of the feature since it remains nearly equal to 1.81 and 1.78, respectively, and for all values of ε. That is, as predicted by the theory since the estimator is both reliable (Theorem 4.3) and efficient up to oscillations (Theorem 4.4), here in dimension two, the dependence of the estimator with respect to the size of the feature is explicit.

Let us now consider two-dimensional examples of geometries with a positive feature. Let Ω_0, Γ_D, f, h and g be as before, and let $\Omega_\varepsilon^j := \mathrm{int}\left(\overline{\Omega_0} \cup \overline{F_\varepsilon^j}\right)$ for $j = 3, 4$ with

$$F_\varepsilon^3 := \left\{ \left(0.5 + r\cos(\theta), 1 + r\sin(\theta)\right) \in \mathbb{R}^2 : 0 \le r < \varepsilon, 0 < \theta < \pi \right\},$$
$$F_\varepsilon^4 := (1 - \varepsilon, 1) \times (1, 1 + \varepsilon),$$

as in Fig. 8c and Fig. 8d. Let $\Gamma_N := \partial\Omega_\varepsilon^j \setminus \overline{\Gamma_D}$. For each $j = 3, 4$, we consider the same Poisson problem (1) as before, but solved in Ω_ε^j. We also solve its defeatured version (3) in Ω_0 with $g_0 \equiv 0$ on $\partial\Omega_0 \setminus \partial\Omega_\varepsilon^j$. Then we extend the defeatured solution to F_ε^j by (6) with $\tilde{F} := F_\varepsilon^j$. We respectively call $u^{(j)}$ and $u_0^{(j)}$ the exact and defeatured solutions, and $u_d^{(j)}$ the defeatured solution extended to F_ε^j.

The results are presented in Fig. 9b. As for the negative feature case, the error in Ω_0 and the estimator converge with respect to the size of the feature as $\varepsilon \propto |\gamma_0|$ in the first geometry Ω_ε^3, and as $\varepsilon^2 \propto |\gamma|^2$ in the

(a) Exact domain Ω_ε^5.

(b) Zoom on part of the upper boundary of Ω_0 (up) and Ω_ε^5 (down).

(c) Exact domain Ω_ε^6.

(d) Zoom on part of the upper boundary of Ω_0 (up) and Ω_ε^6 (down).
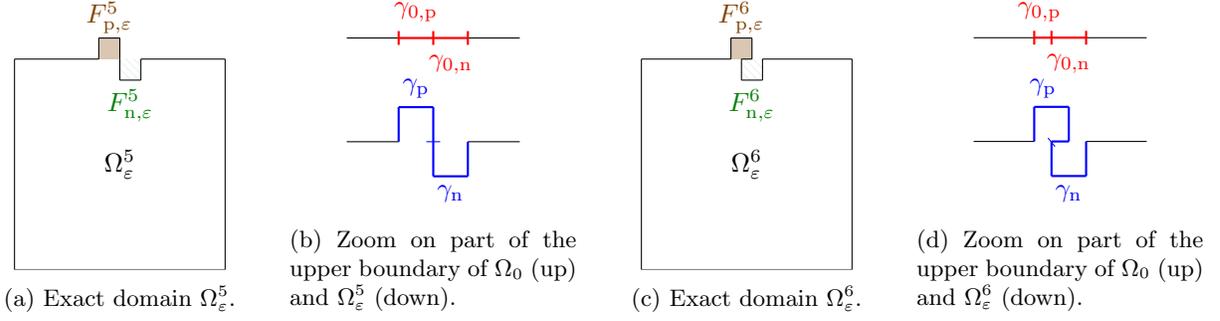
Figure 10: Exact domains Ω_ε^5 and Ω_ε^6.

second geometry Ω_ε^4. Again, the difference in asymptotic behavior of the error depends on symmetries and on the Neumann boundary conditions. Indeed, Ω_ε^4 has features with sides parallel to $\partial\Omega_0$. Moreover, the effectivity index is indeed almost independent from the size of the feature since it remains nearly equal to 2.93 and 3.22, respectively, for all values of ε. That is, as predicted by the theory since the estimator is both reliable (Theorem 5.5) and efficient up to oscillations (Theorem 5.6), here in dimension two, the dependence of the estimator with respect to the size of the feature is explicit. We also remark that the effectivity indices for the positive features are little bit larger than the ones for the negative features.

Let us finally consider two-dimensional examples of geometries with a general complex feature. Let Ω_0, Γ_D, f, h and g be again as before, and for $\ell = 5, 6$, let $\Omega_\varepsilon^\ell := \mathrm{int}\left(\overline{\Omega_0} \cup \overline{F_{n,\varepsilon}^\ell} \setminus \overline{F_{p,\varepsilon}^\ell}\right)$ where, as illustrated in Fig. 10,

$$F_{p,\varepsilon}^5 := \{(0.5 - \varepsilon, 1) + (r, t) : 0 < r, t < \varepsilon\},$$
$$F_{n,\varepsilon}^5 := \{(0.5, 1) + (r, -t) : 0 < r, t < \varepsilon\},$$
$$F_{p,\varepsilon}^6 := \left\{\left(0.5 - \frac{3\varepsilon}{4}, 1\right) + (r, t) : 0 < r, t < \varepsilon\right\},$$
$$F_{n,\varepsilon}^6 := \left\{\left(0.5 - \frac{\varepsilon}{4}, 1\right) + (r, -t) : 0 < r, t < \varepsilon\right\}.$$

For each $\ell = 5, 6$, let $\Gamma_N := \partial\Omega_\varepsilon^\ell \setminus \overline{\Gamma_D}$ and we consider the same Poisson problem (1) as before, but solved in Ω_ε^ℓ. We also solve its defeatured version (3) in Ω_0 with $g_0 \equiv 0$ on γ_0 (note from Fig. 10 that γ_0 is different whether $\ell = 5$ or $\ell = 6$). Then we extend the defeatured solution to F_ε^ℓ by (6) with $\tilde{F} := F_{n,\varepsilon}^\ell$. As before, we respectively call $u^{(\ell)}$ and $u_0^{(\ell)}$ the exact and defeatured solutions, and $u_d^{(\ell)}$ the defeatured solution extended to $F_{n,\varepsilon}^\ell$.

The results are presented in Fig. 9c. As for the negative and positive feature cases, the error in Ω_0 and the estimator converge with respect to the size of the feature as $\varepsilon \propto |\gamma_n| \simeq |\gamma_{0,p}|$ in both geometries Ω_ε^5 and Ω_ε^6. Moreover, the effectivity index is indeed almost independent from the size of the feature since it remains nearly equal to 1.71 and 1.84, respectively, for all values of ε. That is, as predicted by the theory since the estimator is both reliable (Theorem 5.5) and efficient up to oscillations (Theorem 5.6), here in dimension two, the dependence of the estimator with respect to the size of the feature is explicit. We finally remark that the effectivity indices for the positive features are little bit larger than the ones for the negative features.

(a) Geometry Ω_ε^1 with the negative feature F_ε^1.   (b) Geometry Ω_ε^2 with the negative feature F_ε^2.   (c) Geometry Ω_ε^3 with the positive feature F_ε^3.   (d) Geometry Ω_ε^4 with the positive feature F_ε^4.

Figure 11: 3D geometries Ω_ε^i, $i = 1, 2, 3, 4$.

(a) Geometries Ω_ε^1 and Ω_ε^2 with a negative feature.   (b) Geometries Ω_ε^3 and Ω_ε^4 with a positive feature.
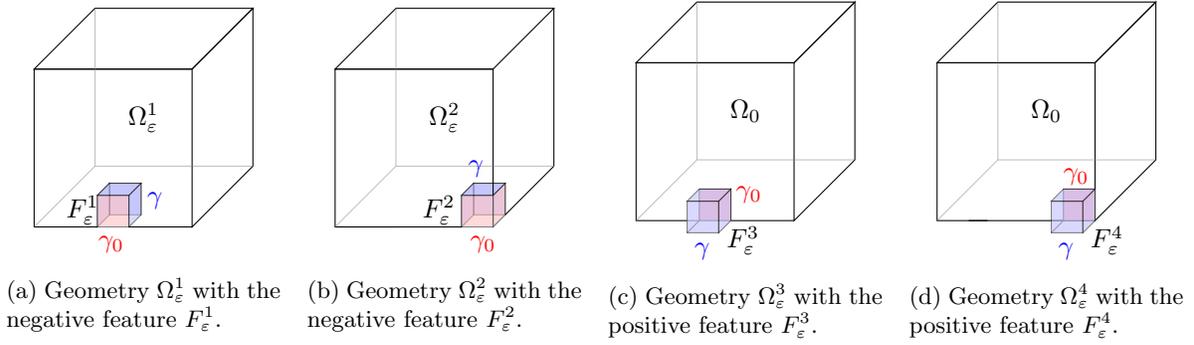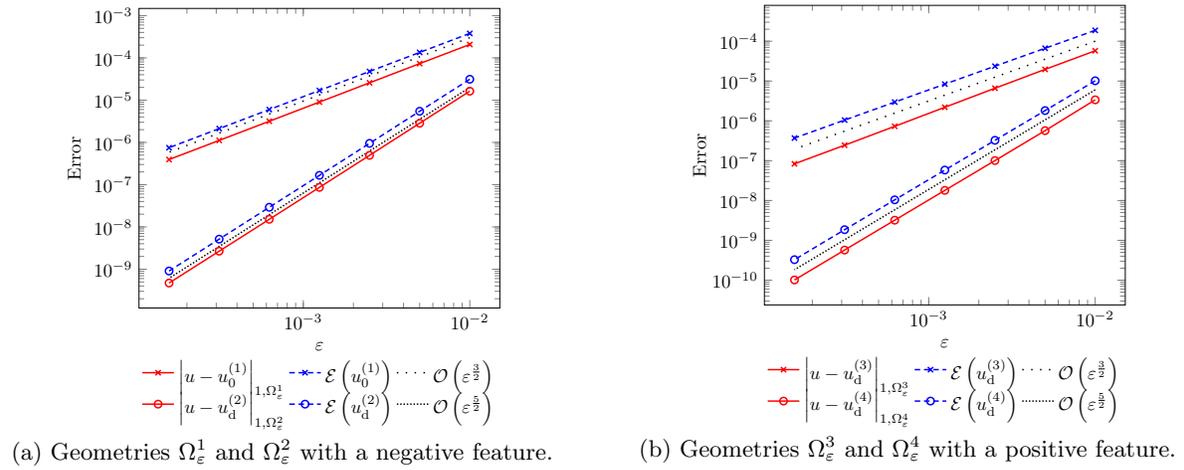
Figure 12: Convergence of the error and of the estimator in 3D domains with one feature.

6.2.2 Three-dimensional geometries

Let us first consider three-dimensional examples of geometries with a negative feature. Let $\varepsilon = \dfrac{10^{-2}}{2^k}$ for $k = 0, 1, \ldots, 6$, and $\Omega_\varepsilon^i := \Omega_0 \setminus \overline{F_\varepsilon^i}$ for $i = 1, 2$ with $\Omega_0 := (0, 1)^3$ and

$$F_\varepsilon^1 := \left\{ (x, y, z) \in \mathbb{R}^3 : 0.5 - \frac{\varepsilon}{2} < x < 0.5 + \frac{\varepsilon}{2}, 1 - \varepsilon < y < 1, 0 < z < \varepsilon \right\},$$
$$F_\varepsilon^2 := F_\varepsilon^1 + \left(0.5 - \frac{\varepsilon}{2}, 0, 0 \right),$$

as in Fig. 11a and Fig. 11b. For each $i = 1, 2$, we consider Poisson problem (1) solved in Ω_ε^i, and its defeatured version (3) in Ω_0. We take

$$f(x, y) := 10 \cos(3\pi x) \sin(5\pi y) \sin(7\pi z) \text{ in } \Omega,$$
$$h \equiv 0 \text{ on } \Gamma_D := \left\{ (x, 0, z) \in \mathbb{R}^3 : 0 < x, z < 1 \right\},$$

$g \equiv 0$ on $\Gamma_N := \partial\Omega_\varepsilon^i \setminus \overline{\Gamma_D}$, and $g_0 \equiv 0$ on $\partial\Omega_0 \setminus \partial\Omega_\varepsilon^i$.

The results are presented in Fig. 12a. Both the error and the estimator converge with respect to the size of the feature as $\varepsilon^{\frac{3}{2}} \propto |\gamma_0|^{\frac{3}{4}}$ in the first geometry Ω_ε^1, and as $\varepsilon^{\frac{5}{2}} \propto |\gamma|^{\frac{5}{4}}$ in the second geometry Ω_ε^2. Moreover, the effectivity index is indeed independent from the size of the feature since it remains nearly equal to 1.87 and 1.92, respectively, for all values of ε. That is, again as predicted by the theory since the estimator is both

reliable (Theorem 4.3) and efficient up to oscillations (Theorem 4.4), here in dimension three, the dependence of the estimator with respect to the size of the feature is explicit.

Let us now consider three-dimensional examples of geometries with a positive feature. Let Ω_0, Γ_D, f, h, and g be as before, and let $\Omega_\varepsilon^j := \mathrm{int}\left(\overline{\Omega_0} \cup \overline{F_\varepsilon^j}\right)$ for $j = 3, 4$ with

$$F_\varepsilon^3 := \left\{(x, y, z) \in \mathbb{R}^3 : 0.5 - \frac{\varepsilon}{2} < x < 0.5 + \frac{\varepsilon}{2}, 1 < y < 1 + \varepsilon, 0 < z < \varepsilon\right\},$$
$$F_\varepsilon^4 := F_\varepsilon^3 + \left(0.5 - \frac{\varepsilon}{2}, 0, 0\right),$$

as in Fig. 11c and Fig. 11d. Let $\Gamma_N := \partial\Omega_\varepsilon^j \setminus \overline{\Gamma_D}$. For each $j = 3, 4$, we consider the same Poisson problem (1) as before, but solved in this Ω_ε^j. We also solve its defeatured version (3) in Ω_0 with $g_0 \equiv 0$ on $\partial\Omega_0 \setminus \partial\Omega_\varepsilon$. Then we extend the defeatured solution to F_ε^j by (6) with $\tilde{F} := F_\varepsilon^j$.

The results are presented in Fig. 12b. As for the negative feature case, the error in Ω_0, the error in F_ε^j and the estimator converge with respect to the size of the feature as $\varepsilon^{\frac{3}{2}} \propto |\gamma_0|^{\frac{3}{4}}$ in the first geometry Ω_ε^3, and as $\varepsilon^{\frac{5}{2}} \propto |\gamma_0|^{\frac{5}{4}}$ in the second geometry Ω_ε^4. Moreover, the effectivity index is indeed almost independent from the size of the feature since it remains nearly equal to 3.10 and 3.22, respectively, for all values of ε. That is, as predicted by the theory since the estimator is both reliable (Theorem 5.5) and efficient up to oscillations (Theorem 5.6), here in dimension three, the dependence of the estimator with respect to the size of the feature is explicit. Finally, and as in the two-dimensional case, we remark that the effectivity indices for the positive features are a little bit larger than the ones for the negative features.

6.2.3 Effect of the choice of the defeatured problem data

Let us study the effect of the choice of the defeatured problem data on the convergence of the defeaturing error and estimator. In particular, we will see that in the example of a geometry with one negative feature F, the convergence of the error and the estimator crucially depends on the value of $\overline{\left(g + \dfrac{\partial u_0}{\partial \mathbf{n}_F}\right)}^\gamma$. As seen in Remark 4.1, this value only depends on the Neumann boundary conditions g on γ and g_0 on γ_0, and on the extension of the right hand side f in F. This means that one can obtain an optimal convergence rate of the defeaturing error by wisely choosing the defeatured data g_0 and f, considering the original data g (if possible, to satisfy the compatibility condition (10)), so that the second term of the estimator in (8) converges faster than the first one. The same observation can be made in the positive feature case.

To show this, let $\varepsilon = \dfrac{10^{-2}}{2^k}$ for $k = 0, 1, \ldots, 6$. We consider a 2D geometry with one negative feature. More precisely, let Ω_0 be the disk centered in $(0, 0)$ of radius 1, let F_ε be the disk centered in $(0, 0)$ of radius ε, and let $\Omega_\varepsilon := \Omega_0 \setminus F_\varepsilon$, as represented in Fig. 6b. We solve Poisson problem (1) in Ω_ε with $f \equiv 1$ in Ω_ε, $h \equiv 0$ on $\Gamma_D := \partial\Omega_0$, and we choose different Neumann data $g = g_i$ on ∂F_ε for $i = 1, \ldots, 4$, where $g_1 \equiv 0$, $g_2 \equiv 1$, $g_3 \equiv \varepsilon^{-1}$, and $g_4 \equiv \varepsilon^{-3}$. Then we solve the defeatured problem (3) in Ω_0, for which we need to choose an extension of f in F_ε, that we still call f. This extension should somehow mimic the behavior of the Neumann data g, as required by the compatibility condition, but instead of that, we choose the trivial extension $f \equiv 1$ in all four cases, and we will verify whether this is always a good choice or not. For $i = 1, \ldots, 4$, we call $u^{(i)}$ and $u_0^{(i)}$ the solutions of (1) and (3), respectively.

The results are presented in Fig. 13. As we can see and as expected, the proposed estimator follows the convergence of the defeaturing error in all four cases. Moreover, the effectivity index always remains the same, as we were also expecting since the shape of the geometry never changes. However, we see that the trivial extension of f in F is not always a good choice since it slows down the convergence when $g = g_2$, it does not permit the error to decrease with ε when $g = g_3$, and it even implies the error to explode with ε when $g = g_4$. The explanation is present in the expression of the estimator in (8): indeed, in the case $g = g_1$, the first term of (8) is dominant, while in the other cases, the second term dominates because of the value of $\overline{\left(g + \dfrac{\partial u_0}{\partial \mathbf{n}_F}\right)}^\gamma$ due to the bad choice of f in F_ε.
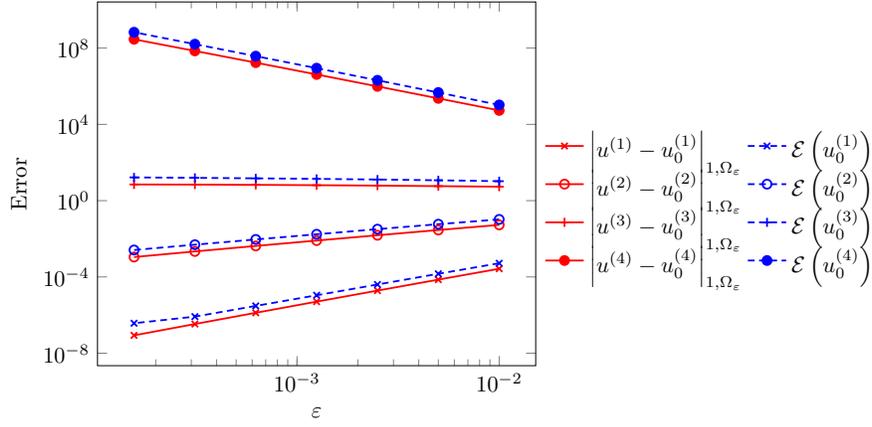
Figure 13: Convergence of the error and of the estimator with different Neumann boundary conditions.

Consequently, the estimator not only tells us whether a feature is important for the given problem at hand, but it also tells us whether the choice of the defeaturing problem data is right or should be reconsidered.

6.3 Non-Lipschitz features: fillets and rounds

Classical features one finds in design for manufacturing are fillets and rounds, that allow for example the use of round-tipped end mills to cut out some material. However, when considered as features isolated from the rest of the domain, fillets and rounds are non-Lipschitz feature domains. The following numerical examples analyze these types of features, and show that our estimator manages to capture the behavior of the defeaturing error even if the domains are not Lipschitz.

6.3.1 Round: a negative non-Lipschitz feature

Let us first consider the case of a round, that is, the rounding process creates a convex domain. For $R \in (0, 1]$, and as represented in Fig. 14, let

$$\Omega_R := (R, 1 - R) + \left\{ \left(r \cos(\theta), r \sin(\theta) \right) \in \mathbb{R}^2 : 0 \le r < R, \, \frac{\pi}{2} < \theta < \pi \right\}$$
$$\cup (0, 1) \times (0, R] \cup [R, 1) \times [1 - R, 1),$$

(a) Geometry Ω_1 with the round feature F_1.

(b) Simplified geometry $\Omega_0 := \Omega_1 \cup F_1$.

(c) Geometry $\Omega_{\frac{1}{2}}$ with the round feature $F_{\frac{1}{2}}$.

(d) Simplified geometry $\Omega_0 := \Omega_{\frac{1}{2}} \cup F_{\frac{1}{2}}$.
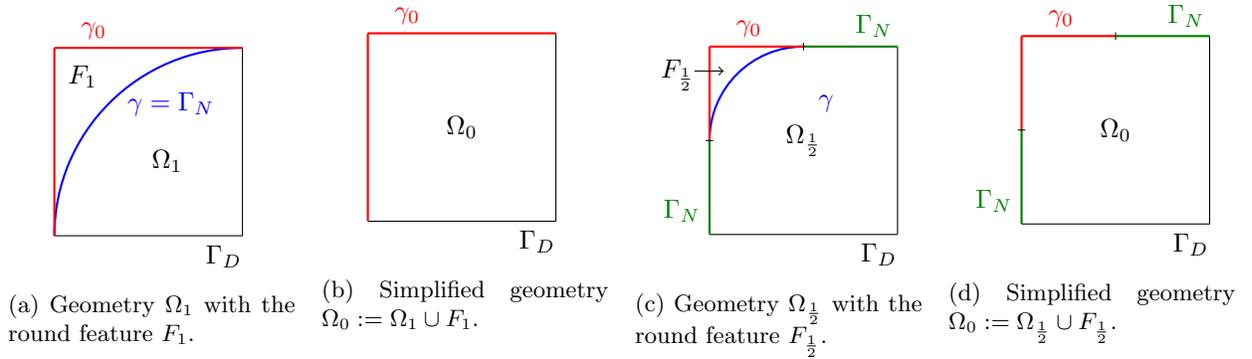
Figure 14: Geometries with a round.

R	$\mathcal{E}(u_0)$	$\left|u - u_0\right|_{1,\Omega_R}$	Effectivity index
1	$6.83 \cdot 10^{-3}$	$2.37 \cdot 10^{-3}$	2.88
0.99	$6.48 \cdot 10^{-3}$	$2.27 \cdot 10^{-3}$	2.85
0.5	$3.36 \cdot 10^{-4}$	$1.26 \cdot 10^{-4}$	2.67
0.25	$2.08 \cdot 10^{-5}$	$7.77 \cdot 10^{-6}$	2.67
0.125	$1.30 \cdot 10^{-6}$	$4.86 \cdot 10^{-7}$	2.67

Table 3: Results for the geometry with a round.

$\Omega_0 := (0,1)^2$, and $F_R := \Omega_0 \backslash \overline{\Omega_R}$. We remark that F_R is not a Lipschitz domain, that is, this case is not covered by the presented theory. We consider Poisson problem (1) with $f \equiv 0$ in Ω_R, $h(x,y) := x^2 \left(1-x\right)^2 + y^2(1-y)^2$ on

$$\Gamma_D := \left\{(x,0),(1,y) \in \mathbb{R}^2 : 0 \leq x, y < 1\right\}.$$

and $g \equiv 0$ on $\Gamma_N := \partial\Omega_R \setminus \overline{\Gamma_D}$. We solve the defeatured Poisson problem (3) with the same data and $g_0 \equiv 0$ on $\gamma_0 := \partial F_R \setminus \overline{\Gamma_N}$.

The results are presented in Table 3, and for all considered values of R, we indeed have $\left|u - u_0\right|_{1,\Omega_R} \lesssim \mathcal{E}(u_0)$ with a low effectivity index. In particular, the effectivity index is almost the same for all considered values of R in $(0, 0.5)$ while it is slightly larger for $R \in (0.5, 1)$, since the geometries for $R \in (0, 0.5)$ are almost an homothety of one another, while it is not when $R > 0.5$ because of the closeness of the boundary Γ_D from the boundary γ. This example shows that our estimator estimates well the defeaturing error even if the feature is not a Lipschitz domain, and it confirms the fact that we can indeed have a feature that is attached to the Dirichlet boundary, that is $\overline{\gamma} \cap \overline{\Gamma_D} \neq \emptyset$ but $\gamma \cap \Gamma_D = \emptyset$, as in the case $R = 1$.

6.3.2 Fillet: a positive non-Lipschitz feature

Now, let us consider the case of a fillet, that is, the filleting process creates a non-convex domain. Since the fillet F is a complex positive feature we possibly do not want to mesh, we will consider two different feature extensions $\tilde{F}^1$ and $\tilde{F}^2$ containing F to solve the extension problem (6). We will compare them, and we will also compare the result with the one obtained without feature extension, that is for $\tilde{F} = F$. In particular, we remark again that F is not a Lipschitz domain, that is, this example is not covered by the presented theory. As illustrated in Fig. 15, let

$$\Omega_0 := (0,1)^2 \setminus \left[\frac{1}{2},1\right]^2, \qquad \tilde{F}^1 := \left(\frac{1}{2},1\right)^2,$$

$$\tilde{F}^2 := \tilde{F}^1 \setminus \left\{\left(1 + r\cos(\theta), 1 + r\sin(\theta)\right) \in \mathbb{R}^2 : 0 \leq r \leq \frac{1}{4}, \pi \leq \theta \leq \frac{3\pi}{2}\right\},$$

$$F := \tilde{F}^1 \setminus \left\{\left(1 + r\cos(\theta), 1 + r\sin(\theta)\right) \in \mathbb{R}^2 : 0 \leq r \leq \frac{1}{2}, \pi \leq \theta \leq \frac{3\pi}{2}\right\},$$

$$\Omega := \text{int}\left(\overline{\Omega_0} \cup \overline{F}\right).$$

$\tilde{F}^1$ is the bounding box of F, it is therefore a very simple geometry but $\left|\tilde{F}^1\right| \gg |F|$. At the contrary, $\tilde{F}^2$ is a little bit more complex, but $\left|\tilde{F}^2\right| \approx |F|$.

We consider Poisson problem (1) with $f \equiv 0$ in Ω,

$$h(x,y) := \cos\left(\pi x\right) + 10\cos(5\pi x)$$

on $\Gamma_D := \left\{(x,0), \in \mathbb{R}^2 : 0 \leq x \leq 1\right\}$, and $g \equiv 0$ on $\Gamma_N = \partial\Omega \setminus \overline{\Gamma_D}$. We solve the defeatured Poisson problem (3) with the same data and with $g_0 \equiv 0$ on $\gamma_0 := \partial\Omega_0 \cap \partial F$. Then, we solve the Dirichlet extension problem

(a) Exact original geometry $\Omega = \mathrm{int}\left(\overline{\Omega_0} \cup \overline{F}\right)$.

(b) Simplified geometry Ω_0 and feature extension $\tilde{F}^1$.

(c) Simplified geometry Ω_0 and feature extension $\tilde{F}^2$.
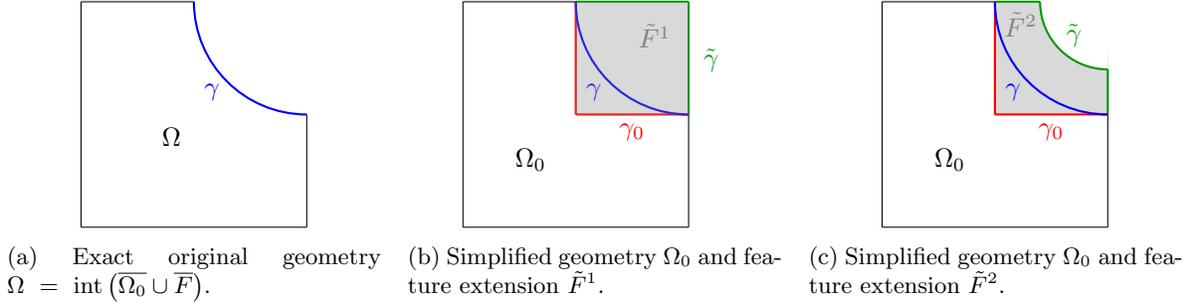
Figure 15: Geometry $\Omega = \mathrm{int}\left(\overline{\Omega_0} \cup \overline{F}\right)$ with a fillet F, and two possible extended features.

Extension	$\mathcal{E}(u_\mathrm{d})$	$\left|u - u_\mathrm{d}\right|_{1,\Omega}$	$\left|u - u_0\right|_{1,\Omega_0}$	$\left|u - \tilde{u}_0\right|_{1,F}$	Effectivity index
$\tilde{F}^1$	$1.78 \cdot 10^0$	$2.92 \cdot 10^{-1}$	$1.69 \cdot 10^{-1}$	$2.39 \cdot 10^{-1}$	6.11
$\tilde{F}^2$	$1.71 \cdot 10^0$	$2.89 \cdot 10^{-1}$	$1.69 \cdot 10^{-1}$	$2.34 \cdot 10^{-1}$	5.93
F	$1.33 \cdot 10^0$	$2.69 \cdot 10^{-1}$	$1.69 \cdot 10^{-1}$	$2.01 \cdot 10^{-1}$	4.94

Table 4: Results for the geometry with a fillet.

(6) first in $\tilde{F}^1$, and secondly in $\tilde{F}^2$, with $\tilde{g} \equiv 0$ on $\tilde{\gamma} := \partial \tilde{F}^1 \setminus \overline{\gamma_0}$ and $\tilde{\gamma} := \partial \tilde{F}^2 \setminus \overline{\gamma_0}$, respectively. Finally, we also solve (6) by taking $\tilde{F} := F$ itself.

The results are presented in Table 4, and we indeed have $\left|u - u_\mathrm{d}\right|_{1,\Omega} \lesssim \mathcal{E}(u_\mathrm{d})$ with a reasonable effectivity index in all three cases. Note that the effectivity index is higher in this case than in the case of a round since not only the geometry Ω but also the feature F are simplified, respectively by Ω_0 and by $\tilde{F}^1$ or $\tilde{F}^2$. Moreover, F contains the extension $\tilde{F}^1$ that itself contains the extension $\tilde{F}^2$, and this is reflected both on the defeaturing error and on the estimator. Indeed, both the error and the estimator are larger when the considered extension is $\tilde{F}^1$ instead of $\tilde{F}^2$, and smaller when $\tilde{F} = F$, but the effectivity index is not affected: it is different because the shapes of F, $\tilde{F}^1$ and $\tilde{F}^2$ are different, not because an extension is bigger than the other one, as we have seen in the numerical examples of Sec. 6.1 and Sec. 6.2. Furthermore, the effectivity index on the fillet is larger than the one on the round: as already remarked in Sec. 6.2, the effectivity index is in general larger for positive features than for negative ones. Finally, the effectivity indices for both the round and the fillet are larger than for the other negative and positive features, respectively, and this can come from the fact that rounds and fillets are non-Lipschitz features.

Remark 6.1 (Effectivity indices) Let us summarize the observations made on the behavior of the effectivity indices.

- The effectivity index of every test case is independent from the measure of the feature (see Sec. 6.2.1 and 6.2.2), but it depends on their shape (see Sec. 6.1.1).

- The observed effectivity indices are small when Lipschitz features are considered: in both two and three dimensions, the value of the effectivity index ranges between 1 and 4 (see Sec. 6.1 and 6.2), in general with smaller values for negative features than for positive ones. While we have no evidence of it, the difference possibly comes from the smoothness of the defeatured solution u_0. Indeed, in the positive feature case, a γ_0-Dirichlet extension of u_0 is necessary to define the error in the whole geometry Ω. This extension is in $H^1(\Omega)$ by definition, but its gradient jumps at the boundary γ_0, making it possibly less regular than the defeatured solution that one can have in the negative feature case.

- The observed effectivity indices are larger when non-Lipschitz features are considered, but such geometries are not considered in the presented theory. The special cases of rounds and fillets are analyzed in Sec. 6.3, and the observed effectivity indices in those cases are smaller than 3 and 5, respectively.

- The observed effectivity indices in the case of an extended positive feature, that is, a feature for which $\tilde{F} \supsetneq F$, are larger than in the case of a positive feature, while still remaining relatively small (see Sec. 6.3.2). Indeed, in the former case, not only the geometry Ω but also the feature F are simplified, respectively by Ω_0 and by $\tilde{F}$.

7 Conclusions

We have introduced a novel *a posteriori* error estimator for analysis-aware geometric defeaturing in the context of Poisson equation on geometries of arbitrary dimension. We have demonstrated its reliability and efficiency up to oscillations, and tested it on an extensive set of numerical experiments: in all of them, we have observed that the proposed estimator acts as an excellent approximation of the true error. We have considered geometries with either a negative, a positive or a general complex feature, and we have verified that our estimator is not only driven by geometrical considerations, but also by the differential problem at hand. The proposed estimator is able to weight the impact of defeaturing in energy norm, and it is explicit with respect to the size of the geometrical features. Finally, our estimator is simple and computationally cheap: once the solution of the defeatured problem is computed, it only requires the computation of the solution of a local extension problem if the feature has a positive component, and of boundary integrals.

In this paper, the analysis is performed in continuous spaces, and for one feature only. The extension to a few features is not hard as the indicator is merely additive, but the extension to several features as well as the development of a fully adaptive scheme taking into account the discretization and the defeaturing errors will be the object of our subsequent work. Finally, this work focuses on the global energy norm of the error, which is an important first step to understand the impact of defeaturing in analysis. Studying defeaturing using a local goal-oriented error measure would be a further step attracting a broader industrial interest.

A Appendix

In this section, we state lemmas that are used throughout the paper, and the symbol $\lesssim$ will be used to mean any inequality which does not depend on the size of the considered domains, but which can depend on their shape. We assume that all considered domains are Lipschitz.

Appendix A.1 (Poincaré I) Let ω be an $(n-1)$-dimensional manifold in $\mathbb{R}^n$ that is isotropic according to Definition 2.1. Then for all $v \in H^{\frac{1}{2}}(\omega)$,

$$\|v - \overline{v}\|_{0,\omega} \lesssim |\omega|^{\frac{1}{2(n-1)}} |v|_{\frac{1}{2},\omega},$$

where $\overline{v} := \frac{1}{|\omega|} \int_\omega v \, \mathrm{d}s$ is the average of v on ω.

Proof. Let $v \in H^{\frac{1}{2}}(\omega)$. Recall that since ω is an $(n-1)$-dimensional manifold in $\mathbb{R}^n$, then

$$|v|_{\frac{1}{2},\omega}^2 = \int_\omega \int_\omega \frac{\big(v(x) - v(y)\big)^2}{|x-y|^n} \, \mathrm{d}x \, \mathrm{d}y.$$

Moreover, let

$$\omega_{\max} := \arg \max_{\omega_c \in \mathrm{conn}(\omega)} \big(\mathrm{diam}\,(\omega_c)\big).$$

Then since ω is isotropic,

$$\mathrm{diam}\,(\omega) \lesssim \mathrm{diam}\,(\omega_{\max}) \lesssim |\omega_{\max}|^{\frac{1}{n-1}} \leq |\omega|^{\frac{1}{n-1}}.$$

Therefore,

$$
\begin{aligned}
\|v - \bar{v}\|_{0,\omega}^2 &= \int_\omega \left(v(x) - \frac{1}{|\omega|} \int_\omega v(y)\, \mathrm{d}y \right)^2 \mathrm{d}x \\
&= \frac{1}{|\omega|^2} \int_\omega \left[\int_\omega \left(v(x) - v(y) \right) \mathrm{d}y \right]^2 \mathrm{d}x \\
&\leq \frac{1}{|\omega|^2} \int_\omega \left[|\omega| \int_\omega \left(v(x) - v(y) \right)^2 \mathrm{d}y \right] \mathrm{d}x \\
&= \frac{1}{|\omega|} \int_\omega \int_\omega \frac{\left(v(x) - v(y) \right)^2}{|x - y|^n} |x - y|^n\, \mathrm{d}y\, \mathrm{d}x \\
&\leq \frac{\mathrm{diam}\,(\omega)^n}{|\omega|} \int_\omega \int_\omega \frac{\left(v(x) - v(y) \right)^2}{|x - y|^n}\, \mathrm{d}y\, \mathrm{d}x \lesssim |\omega|^{\frac{1}{n-1}} |v|_{\frac{1}{2},\omega}^2.
\end{aligned}
$$

$\square$

Appendix A.2 Let $D \subset \mathbb{R}^n$, and let $\omega \subset \partial D$ be a $(n-1)$-dimensional manifold in $\mathbb{R}^n$. Then for all $v \in H^{\frac{1}{2}}(\partial D)$, if we define $\eta \in \mathbb{R}$ as the unique solution of $\eta = -\log(\eta)$,

$$
\|v\|_{0,\omega} \lesssim c_\omega |\omega|^{\frac{1}{2(n-1)}} \|v\|_{\frac{1}{2},\partial D}, \quad \text{where} \quad c_\omega := \begin{cases} \max\left(|\log(|\omega|)|, \eta \right)^{\frac{1}{2}} & \text{if } n = 2; \\ 1 & \text{if } n = 3. \end{cases}
$$

The hidden constant is independent from the measure of ω.

Proof. Let $v \in H^{\frac{1}{2}}(\partial D)$. By Sobolev embedding, it is well known that $H^{\frac{1}{2}}(\partial D)$ can be continuously embedded in $L^{2p}(\partial D)$ for every $1 \leq p < \infty$ if $n = 2$, or for every $1 \leq p \leq 2$ if $n = 3$. Therefore, by Hölder inequality,

$$
\|v\|_{0,\omega}^2 = \sum_{\omega_c \in \mathrm{conn}(\omega)} \|v\|_{0,\omega_c}^2 \leq \sum_{\omega_c \in \mathrm{conn}(\omega)} |\omega_c|^{1-\frac{1}{p}} \|v\|_{L^{2p}(\omega_c)}^2 \lesssim |\omega|^{1-\frac{1}{p}} \|v\|_{L^{2p}(\partial D)}^2. \tag{43}
$$

If $n = 3$, by taking $p = 2$ in (43) and by Sobolev embedding,

$$
\|v\|_{0,\omega}^2 \lesssim |\omega|^{\frac{1}{2}} \|v\|_{\frac{1}{2},\partial D}^2 = c_\omega^2 |\omega|^{\frac{1}{n-1}} \|v\|_{\frac{1}{2},\partial D}^2.
$$

Let us now consider the case $n = 2$. Thanks to Ref. [49, Lemma 5.1], it is known that for all $q \in [2, \infty)$ and all $v \in H^{\frac{1}{2}}(0, 2\pi)$,

$$
\|v\|_{L^q(0,2\pi)} \leq c \sqrt{q} \|v\|_{\frac{1}{2},(0,2\pi)},
$$

where c is a constant independent from q. Then by definition of the norms L^q and $H^{\frac{1}{2}}$ on a manifold (see Ref. [44, Sec. 1.3.3]), we obtain $\|v\|_{L^{2p}(\partial D)} \leq \tilde{c}\sqrt{p}\|v\|_{\frac{1}{2},\partial D}$, where $\tilde{c}$ is a constant independent from p. So by taking $p = \max\left(|\log(|\omega|)|, \eta \right) = c_\omega^2$ in (43), then $|\omega|^{-\frac{1}{p}} \leq e$ and thus

$$
\|v\|_{0,\omega}^2 \lesssim |\omega|^{1-\frac{1}{p}} p \|v\|_{\frac{1}{2},\partial D}^2 \lesssim |\omega| c_\omega^2 \|v\|_{\frac{1}{2},\partial D}^2 = c_\omega^2 |\omega|^{\frac{1}{n-1}} \|v\|_{\frac{1}{2},\partial D}^2.
$$

$\square$

Appendix A.3 (Poincaré II) Let ω be an $(n-1)$-dimensional manifold in $\mathbb{R}^n$ that is isotropic according to Definition 2.1. Then for all $v \in H_{00}^{\frac{1}{2}}(\omega)$,

$$
\|v\|_{0,\omega} \lesssim |\omega|^{\frac{1}{2(n-1)}} \|v\|_{H_{00}^{1/2}(\omega)}.
$$

Proof. Let $D \subset \mathbb{R}^n$ and $\varphi \subset \mathbb{R}^n$ such that $\partial D = \overline{\omega} \cup \overline{\varphi}$ and $\omega \cap \varphi = \emptyset$. Let $v \in H_{00}^{\frac{1}{2}}(\omega)$. First, suppose that ω is connected. Then from Ref. [50, Proposition 2.4], since ω is isotropic and if we let $v^\star \in H^{\frac{1}{2}}(\partial D)$ be the extension of v by 0,

$$\|v\|_{0,\omega}^2 \lesssim |\omega|^{\frac{1}{n-1}} |v^\star|_{\frac{1}{2},\partial D}^2 \leq |\omega|^{\frac{1}{n-1}} \|v^\star\|_{\frac{1}{2},\partial D}^2 = |\omega|^{\frac{1}{n-1}} \|v\|_{H_{00}^{1/2}(\omega)}^2. \tag{44}$$

Now, if ω is not connected, then $\mathrm{dist}(s, \partial \omega_c) = \mathrm{dist}(s, \partial \omega)$ for all $\omega_c \in \mathrm{conn}(\omega)$ and for all $s \in \omega_c$. Thus

$$\sum_{\omega_c \in \mathrm{conn}(\omega)} \|v|_{\omega_c}\|_{H_{00}^{1/2}(\omega_c)}^2 = \sum_{\omega_c \in \mathrm{conn}(\omega)} \left(\|v|_{\omega_c}\|_{\frac{1}{2},\omega_c}^2 + |v|_{\omega_c}|_{H_{00}^{1/2}(\omega_c)}^2 \right)$$

$$\lesssim \|v\|_{\frac{1}{2},\omega}^2 + \sum_{\omega_c \in \mathrm{conn}(\omega)} \int_{\omega_c} \frac{v^2(s)}{\mathrm{dist}(s, \partial \omega_c)} \, \mathrm{d}s$$

$$= \|v\|_{\frac{1}{2},\omega}^2 + \int_{\omega} \frac{v^2(s)}{\mathrm{dist}(s, \partial \omega)} \, \mathrm{d}s = \|v\|_{H_{00}^{1/2}(\omega)}^2.$$

Therefore, from (44),

$$\|v\|_{0,\omega}^2 = \sum_{\omega_c \in \mathrm{conn}(\omega)} \|v\|_{0,\omega_c}^2 \lesssim \sum_{\omega_c \in \mathrm{conn}(\omega)} |\omega_c|^{\frac{1}{n-1}} \|v\|_{H_{00}^{1/2}(\omega_c)}^2 \lesssim |\omega|^{\frac{1}{n-1}} \|v\|_{H_{00}^{1/2}(\omega)}^2.$$

$\square$

Appendix A.4 Let ω be an $(n-1)$-dimensional manifold in $\mathbb{R}^n$ that is isotropic according to Definition 2.1. Then for all $v \in L^2(\omega)$,

$$\|v\|_{H_{00}^{-1/2}(\omega)} \lesssim |\omega|^{\frac{1}{2(n-1)}} \|v\|_{0,\omega}.$$

Proof. Since $H_{00}^{-\frac{1}{2}}(\omega)$ is the dual space of $H_{00}^{\frac{1}{2}}(\omega)$, then by Appendix A.3, we obtain

$$\|v\|_{H_{00}^{-1/2}(\omega)} = \sup_{\substack{z \in H_{00}^{1/2}(\omega) \\ z \neq 0}} \frac{\displaystyle\int_{\omega} vz \, \mathrm{d}s}{\|z\|_{H_{00}^{1/2}(\omega)}}$$

$$\leq \sup_{\substack{z \in H_{00}^{1/2}(\omega) \\ z \neq 0}} \frac{\|v\|_{0,\omega} \|z\|_{0,\omega}}{\|z\|_{H_{00}^{1/2}(\omega)}}$$

$$\lesssim \sup_{\substack{z \in H_{00}^{1/2}(\omega) \\ z \neq 0}} \frac{\|v\|_{0,\omega} |\omega|^{\frac{1}{2(n-1)}} \|z\|_{H_{00}^{1/2}(\omega)}}{\|z\|_{H_{00}^{1/2}(\omega)}} = |\omega|^{\frac{1}{2(n-1)}} \|v\|_{0,\omega}.$$

$\square$

Appendix A.5 (Inverse inequality I) Let ω be an open $(n-1)$-dimensional manifold in $\mathbb{R}^n$ that is isotropic and regular according to Definitions 2.1 and 2.2, and let $m \in \mathbb{N}$. Then for all $p \in \mathbb{Q}_{m,0}^{\mathrm{pw}}(\omega)$,

$$\|p\|_{0,\omega} \lesssim |\omega|^{-\frac{1}{2(n-1)}} \|p\|_{H_{00}^{-1/2}(\omega)},$$

where the hidden constant increases with m.

Proof. For all $q \in \mathbb{Q}_{m,0}^{\mathrm{pw}}(\omega) \subset H_0^1(\omega)$, the following inverse estimate is well known (see Ref. [51, Theorem 3.2] for example): with the notation of Definition 2.2, for all $\ell = 1, \ldots, L_\omega$,

$$|q|_{\omega_\ell}|_{1,\omega_\ell} \lesssim |\omega_\ell|^{-\frac{1}{n-1}} \|q|_{\omega_\ell}\|_{0,\omega_\ell},$$

and the hidden constant increases with m. Therefore, since ω is isotropic and shape regular,

$$|q|_{1,\omega} \lesssim \max_{\ell=1,\ldots,L_\omega} \left(|\omega_\ell|^{-\frac{1}{n-1}}\right) \|q\|_{0,\omega} \lesssim |\omega|^{-\frac{1}{n-1}} \|q\|_{0,\omega}.$$

Moreover, from Ref. [52], we know that the interpolation space

$$\left[H_0^1\left(\omega\right), L^2\left(\omega\right)\right]_{\frac{1}{2}} = H_{00}^{\frac{1}{2}}\left(\omega\right)$$

(see also Ref. [53, Theorem 11.7]). Therefore, from Ref. [53, Proposition 2.3], for all $q \in \mathbb{Q}_{m,0}^{\mathrm{pw}}(\omega)$,

$$\|q\|_{H_{00}^{1/2}(\omega)} \lesssim |q|_{1,\omega}^{\frac{1}{2}} \|q\|_{0,\omega}^{\frac{1}{2}} \lesssim |\omega|^{-\frac{1}{2(n-1)}} \|q\|_{0,\omega}. \tag{45}$$

Consequently, for all $p \in \mathbb{Q}_{m,0}^{\mathrm{pw}}(\omega) \subset H_{00}^{-\frac{1}{2}}(\omega)$, since $\mathbb{Q}_{m,0}^{\mathrm{pw}}(\omega) \subset H_{00}^{\frac{1}{2}}(\omega)$,

$$
\begin{aligned}
\|p\|_{0,\omega} = \frac{\displaystyle\int_\omega p^2\,\mathrm{d}s}{\|p\|_{0,\omega}} &\leq \sup_{\substack{q\in\mathbb{Q}_{m,0}^{\mathrm{pw}}(\omega)\\q\neq 0}} \frac{\displaystyle\int_\omega pq\,\mathrm{d}s}{\|q\|_{0,\omega}} \lesssim |\omega|^{-\frac{1}{2(n-1)}} \sup_{\substack{q\in\mathbb{Q}_{m,0}^{\mathrm{pw}}(\omega)\\q\neq 0}} \frac{\displaystyle\int_\omega pq\,\mathrm{d}s}{\|q\|_{H_{00}^{1/2}(\omega)}} \\
&\leq |\omega|^{-\frac{1}{2(n-1)}} \sup_{\substack{v\in H_{00}^{1/2}(\omega)\\v\neq 0}} \frac{\displaystyle\int_\omega pv\,\mathrm{d}s}{\|v\|_{H_{00}^{1/2}(\omega)}} \\
&= |\omega|^{-\frac{1}{2(n-1)}} \|p\|_{H_{00}^{-1/2}(\omega)}. \tag{46}
\end{aligned}
$$

$\square$

For the following lemmas, let $D \subset \mathbb{R}^n$ be an open bounded domain, and let $\partial D = \bigcup_{k=1}^{K+1} \overline{\omega_k}$ for some $K \in \mathbb{N}$, such that $\omega_i \cap \omega_j = \emptyset$, for all $i,j = 1,\ldots,K+1$, and let $\omega = \mathrm{int}\left(\bigcup_{k=1}^{K} \overline{\omega_k}\right)$. Moreover, let

$$H := \left\{v \in H_{00}^{\frac{1}{2}}(\omega) : v|_{\omega_k} \in H_{00}^{\frac{1}{2}}(\omega_k), \forall k = 1,\ldots,K\right\} \subset H_{00}^{\frac{1}{2}}(\omega)$$

equipped with the norm $\|\cdot\|_H := \left(\sum_{k=1}^{K} \|\cdot|_{\omega_k}\|_{H_{00}^{\frac{1}{2}}(\omega_k)}^2\right)^{\frac{1}{2}}$, and let H^* be its dual space, equipped with the dual norm $\|\cdot\|_{H^*}$.

Appendix A.6 For all $v \in H$,

$$\|v\|_{H_{00}^{1/2}(\omega)} \leq \sqrt{K}\|v\|_H,$$

and for all $w \in H_{00}^{-\frac{1}{2}}(\omega)$,

$$\|w\|_{H^*} \leq \sqrt{K}\|w\|_{H_{00}^{-1/2}(\omega)}.$$

Proof. Let $v \in H \subset H_{00}^{\frac{1}{2}}(\omega)$, and let $v|_{\omega_k}^\star$ be the extension of $v|_{\omega_k}$ by 0 on ∂D. Then by triangular inequality,

$$
\begin{aligned}
\|v\|_{H_{00}^{1/2}(\omega)} = \left\|\sum_{k=1}^{K} v|_{\omega_k}^\star\right\|_{H_{00}^{1/2}(\omega)} &\leq \sum_{k=1}^{K} \left\|v|_{\omega_k}^\star\right\|_{H_{00}^{1/2}(\omega)} = \sum_{k=1}^{K} \left\|v|_{\omega_k}^\star\right\|_{\frac{1}{2},\partial D} \\
&= \sum_{k=1}^{K} \left\|v|_{\omega_k}^\star\right\|_{H_{00}^{1/2}(\omega_k)} \leq \sqrt{K}\|v\|_H. \tag{47}
\end{aligned}
$$

Moreover, for all $w \in H_{00}^{-\frac{1}{2}}(\omega) \subset H^*$, using (47),

$$\|w\|_{H^*} = \sup_{\substack{v \in H \\ v \neq 0}} \frac{\int_\omega wv\,\mathrm{d}s}{\|v\|_H} \leq \sqrt{K} \sup_{\substack{v \in H \\ v \neq 0}} \frac{\int_\omega wv\,\mathrm{d}s}{\|v\|_{H_{00}^{1/2}(\omega)}}$$

$$\leq \sqrt{K} \sup_{\substack{v \in H_{00}^{\frac{1}{2}}(\omega) \\ v \neq 0}} \frac{\int_\omega wv\,\mathrm{d}s}{\|v\|_{H_{00}^{1/2}(\omega)}} = \sqrt{K}\|w\|_{H_{00}^{-1/2}(\omega)}.$$

$\square$

Appendix A.7 (Inverse inequality II) Assume that ω is isotropic and regular according to Definitions 2.1 and 2.2, and let $m \in \mathbb{N}$. Then for all piecewise polynomial $p \in \mathbb{Q}_m^0$, where

$$\mathbb{Q}_m^0 := \left\{ q \in \mathbb{Q}_{m,0}^{\mathrm{pw}}(\omega) : q|_{\omega_k} \in \mathbb{Q}_{m,0}^{\mathrm{pw}}(\omega_k), \forall k = 1, \dots, K \right\} \subset H,$$

then

$$\|p\|_{0,\omega} \lesssim |\omega|^{-\frac{1}{2(n-1)}} \|p\|_{H^*},$$

where the hidden constant increases with m.

Proof. For all $q \in \mathbb{Q}_m^0$ and all $k = 1, \dots, K$, $q|_{\omega_k} \in \mathbb{Q}_{m,0}^{\mathrm{pw}}(\omega_k)$, and thus from (45) and since ω is regular,

$$\left\|q|_{\omega_k}\right\|_{H_{00}^{1/2}(\omega_k)} \lesssim |\omega_k|^{-\frac{1}{2(n-1)}} \left\|q|_{\omega_k}\right\|_{0,\omega_k} \lesssim |\omega|^{-\frac{1}{2(n-1)}} \left\|q|_{\omega_k}\right\|_{0,\omega_k}.$$

Therefore,

$$\|q\|_H = \left(\sum_{k=1}^K \left\| \cdot |_{\omega_k} \right\|_{H_{00}^{\frac{1}{2}}(\omega_k)}^2 \right)^{\frac{1}{2}} \lesssim |\omega|^{-\frac{1}{2(n-1)}} \|q\|_{0,\omega}.$$

Consequently, for all $p \in \mathbb{Q}_m^0 \subset H$, following the same steps as in (46) of the proof of Appendix A.5, replacing $H_{00}^{-\frac{1}{2}}(\omega)$ by H^*, $H_{00}^{\frac{1}{2}}(\omega)$ by H, and $\mathbb{Q}_{m,0}^{\mathrm{pw}}(\omega)$ by $\mathbb{Q}_m^0$, then

$$\|p\|_{0,\omega} \lesssim |\omega|^{-\frac{1}{2(n-1)}} \|p\|_{H^*}.$$

$\square$

Acknowledgment

References

[1] R. T. Farouki, "Closing the gap between CAD model and downstream application," *SIAM news*, vol. 32, no. 5, pp. 303–319, 1999.

[2] R. F. Riesenfeld, R. Haimes, and E. Cohen, "Initiating a CAD renaissance: Multidisciplinary analysis driven design: Framework for a new generation of advanced computational design, engineering and manufacturing environments," *Computer Methods in Applied Mechanics and Engineering*, vol. 284, pp. 1054–1072, 2015. Isogeometric analysis special issue.

[3] J. A. Cottrell, T. J. R. Hughes, and Y. Bazilevs, *Isogeometric analysis: towards integration of CAD and FEA*. Wiley, 2009.

[4] T. J. R. Hughes, J. A. Cottrell, and Y. Bazilevs, "Isogeometric analysis: CAD, finite elements, NURBS, exact geometry, and mesh refinement," *Computer Methods in Applied Mechanics and Engineering*, vol. 194, pp. 4135–4195, 2005.

[5] T. J. R. Hughes, "Isogeometric analysis: Progress and challenges," *Computer Methods in Applied Mechanics and Engineering*, vol. 316, p. 1, 2017. Special Issue on Isogeometric Analysis: Progress and Challenges.

[6] Y. Bazilevs, L. Beirão da Veiga, J. A. Cottrell, T. J. R. Hughes, and G. Sangalli, "Isogeometric analysis: approximation, stability and error estimates for h-refined meshes," *Mathematical Models and Methods in Applied Sciences*, vol. 16, no. 07, pp. 1031–1090, 2006.

[7] L. Beirão da Veiga, A. Buffa, G. Sangalli, and R. Vázquez, "Mathematical analysis of variational isogeometric methods," *Acta Numerica*, vol. 23, p. 157–287, 2014.

[8] L. Beirão da Veiga, A. Buffa, G. Sangalli, and R. Vázquez, "Analysis-suitable T-splines of arbitrary degree: definition, linear independence and approximation properties," *Mathematical Models and Methods in Applied Sciences*, vol. 23, no. 11, pp. 1979–2003, 2013.

[9] A. Buffa and E. M. Garau, "A posteriori error estimators for hierarchical B-spline discretizations," *Mathematical Models and Methods in Applied Sciences*, vol. 28, no. 08, pp. 1453–1480, 2018.

[10] A. Buffa and C. Giannelli, "Adaptive isogeometric methods with hierarchical splines: error estimator and convergence," *Mathematical Models and Methods in Applied Sciences*, vol. 26, no. 01, pp. 1–25, 2016.

[11] A. Buffa and C. Giannelli, "Adaptive isogeometric methods with hierarchical splines: optimality and convergence rates," *Mathematical Models and Methods in Applied Sciences*, vol. 27, no. 14, pp. 2781–2802, 2017.

[12] A. Buffa, R. H. Vázquez, G. Sangalli, and L. Beirão da Veiga, "Approximation estimates for isogeometric spaces in multipatch geometries," *Numerical Methods for Partial Differential Equations*, vol. 31, no. 2, pp. 422–438, 2015.

[13] P. Antolin, A. Buffa, and M. Martinelli, "Isogeometric analysis on V-reps: first results," *Computer Methods in Applied Mechanics and Engineering*, vol. 355, pp. 976–1002, 2019.

[14] B. Marussig and T. J. R. Hughes, "A review of trimming in isogeometric analysis: Challenges, data exchange and simulation aspects," *Archives of Computational Methods in Engineering*, vol. 25, pp. 1059–1127, Nov 2018.

[15] R. Schmidt, R. Wüchner, and K.-U. Bletzinger, "Isogeometric analysis of trimmed NURBS geometries," *Computer Methods in Applied Mechanics and Engineering*, vol. 241-244, pp. 93 – 111, 2012.

[16] P. Antolin, A. Buffa, R. Puppi, and X. Wei, "Overlapping multipatch isogeometric method with minimal stabilization," *SIAM Journal on Scientific Computing*, vol. 43, no. 1, pp. A330–A354, 2021.

[17] S. Kargaran, B. Jüttler, S. Kleiss, A. Mantzaflaris, and T. Takacs, "Overlapping multi-patch structures in isogeometric analysis," *Computer Methods in Applied Mechanics and Engineering*, vol. 356, pp. 325 – 353, 2019.

[18] B.-Q. Zuo, Z.-D. Huang, Y.-W. Wang, and Z.-J. Wu, "Isogeometric analysis for CSG models," *Computer Methods in Applied Mechanics and Engineering*, vol. 285, pp. 102 – 124, 2015.

[19] M. Breitenberger, A. Apostolatos, B. Philipp, R. Wüchner, and K.-U. Bletzinger, "Analysis in computer aided design: Nonlinear isogeometric B-Rep analysis of shell structures," *Computer Methods in Applied Mechanics and Engineering*, vol. 284, pp. 401–457, 2015.

[20] L. Coradello, P. Antolin, R. Vázquez, and A. Buffa, "Adaptive isogeometric analysis on two-dimensional trimmed domains based on a hierarchical approach," *Computer Methods in Applied Mechanics and Engineering*, vol. 364, p. 112925, 2020.

[21] T. Teschemacher, A. Bauer, T. Oberbichler, M. Breitenberger, R. Rossi, R. Wüchner, and K.-U. Bletzinger, "Realization of CAD-integrated shell simulation based on isogeometric B-Rep analysis," *Advanced Modeling and Simulation in Engineering Sciences*, vol. 5, no. 1, p. 19, 2018.

[22] M. Elhaddad, N. Zander, S. Kollmannsberger, A. Shadavakhsh, V. Nübel, and E. Rank, "Finite cell method: High-order structural dynamics for complex geometries," *International Journal of Structural Stability and Dynamics*, vol. 15, no. 07, p. 1540018, 2015.

[23] E. Rank, M. Ruess, S. Kollmannsberger, D. Schillinger, and A. Düster, "Geometric modeling, isogeometric analysis and the finite cell method," *Computer Methods in Applied Mechanics and Engineering*, vol. 249, pp. 104–115, 2012.

[24] D. Schillinger, L. Dede, M. A. Scott, J. A. Evans, M. J. Borden, E. Rank, and T. J. R. Hughes, "An isogeometric design-through-analysis methodology based on adaptive hierarchical refinement of nurbs, immersed boundary methods, and T-spline CAD surfaces," *Computer Methods in Applied Mechanics and Engineering*, vol. 249, pp. 116–150, 2012.

[25] A. Thakur, A. G. Banerjee, and S. K. Gupta, "A survey of CAD model simplification techniques for physics-based simulation applications," *Computer-Aided Design*, vol. 41, no. 2, pp. 65–80, 2009.

[26] L. Fine, L. Remondini, and J.-C. Leon, "Automated generation of FEA models through idealization operators," *International Journal for Numerical Methods in Engineering*, vol. 49, no. 1-2, pp. 83–108, 2000.

[27] N. Rahimi, P. Kerfriden, F. C. Langbein, and R. R. Martin, "CAD model simplification error estimation for electrostatics problems," *SIAM Journal on Scientific Computing*, vol. 40, no. 1, pp. B196–B227, 2018.

[28] R. Ferrandes, P. Marin, J.-C. Léon, and F. Giannini, "A posteriori evaluation of simplification details for finite element model preparation," *Computers & Structures*, vol. 87, no. 1, pp. 73 – 80, 2009.

[29] S. H. Gopalakrishnan and K. Suresh, "Feature sensitivity: a generalization of topological sensitivity," *Finite Elements in Analysis and Design*, vol. 44, no. 11, pp. 696 – 704, 2008.

[30] I. Turevsky, S. H. Gopalakrishnan, and K. Suresh, "Defeaturing: A posteriori error analysis via feature sensitivity," *International journal for numerical methods in engineering*, vol. 76, no. 9, pp. 1379–1401, 2008.

[31] K. K. Choi and N.-H. Kim, *Structural Sensitivity Analysis and Optimization 1: Linear Systems*. Springer Science & Business Media, 2005.

[32] J. Sokolowski and A. Zochowski, "On the topological derivative in shape optimization," *SIAM journal on control and optimization*, vol. 37, no. 4, pp. 1251–1272, 1999.

[33] M. Li, S. Gao, and R. R. Martin, "Estimating the effects of removing negative features on engineering analysis," *Computer-Aided Design*, vol. 43, no. 11, pp. 1402 – 1412, 2011. Solid and Physical Modeling 2011.

[34] R. Becker and R. Rannacher, "An optimal control approach to a posteriori error estimation in finite element methods," *Acta numerica*, vol. 10, pp. 1–102, 2001.

[35] J. T. Oden and S. Prudhomme, "Estimation of modeling error in computational mechanics," *Journal of Computational Physics*, vol. 182, no. 2, pp. 496–515, 2002.

[36] C. Carstensen and S. Sauter, "A posteriori error analysis for elliptic PDEs on domains with complicated structures," *Numer. Math.*, vol. 96, no. 4, pp. 691–721, 2004.

[37] J. Oden and K. S. Vemaganti, "Estimation of local modeling error and goal-oriented adaptive modeling of heterogeneous materials: I. Error estimates and adaptive algorithms," *Journal of Computational Physics*, vol. 164, no. 1, pp. 22 – 47, 2000.

[38] K. Vemaganti, "Modelling error estimation and adaptive modelling of perforated materials," *International Journal for Numerical Methods in Engineering*, vol. 59, no. 12, pp. 1587–1604, 2004.

[39] S. Repin, S. Sauter, and A. Smolianski, "A posteriori error estimation for the Dirichlet problem with account of the error in the approximation of boundary conditions," *Computing*, vol. 70, no. 3, pp. 205–233, 2003.

[40] M. Li and S. Gao, "Estimating defeaturing-induced engineering analysis errors for arbitrary 3D features," *Computer-Aided Design*, vol. 43, no. 12, pp. 1587 – 1597, 2011.

[41] M. Li, S. Gao, and K. Zhang, "A goal-oriented error estimator for the analysis of simplified designs," *Computer Methods in Applied Mechanics and Engineering*, vol. 255, pp. 89 – 103, 2013.

[42] M. Li, S. Gao, and R. R. Martin, "Engineering analysis error estimation when removing finite-sized features in nonlinear elliptic problems," *Computer-Aided Design*, vol. 45, no. 2, pp. 361 – 372, 2013. Solid and Physical Modeling 2012.

[43] K. Zhang, M. Li, and J. Li, "Estimation of impacts of removing arbitrarily constrained domain details to the analysis of incompressible fluid flows," *Communications in Computational Physics*, vol. 20, no. 4, p. 944–968, 2016.

[44] P. Grisvard, *Elliptic Problems in Nonsmooth Domains*. Society for Industrial and Applied Mathematics, 2011.

[45] P. Clément, "Approximation by finite element functions using local regularization," *ESAIM: Mathematical Modelling and Numerical Analysis - Modélisation Mathématique et Analyse Numérique*, vol. 9, no. R2, pp. 77–84, 1975.

[46] C. Bernardi and V. Girault, "A local regularization operator for triangular and quadrilateral finite elements," *SIAM J. Numer. Anal.*, vol. 35, p. 1893–1916, Oct. 1998.

[47] R. Vázquez, "A new design for the implementation of isogeometric analysis in Octave and Matlab: GeoPDEs 3.0," *Computers & Mathematics with Applications*, vol. 72, no. 3, pp. 523–554, 2016.

[48] X. Wei, B. Marussig, P. Antolin, and A. Buffa, "Immersed boundary-conformal isogeometric method for linear elliptic problems," *arXiv:2011.01622*, 2020.

[49] F. Ben Belgacem, A. Buffa, and Y. Maday, "The mortar finite element method for 3D Maxwell equations: first results," *SIAM Journal on Numerical Analysis*, vol. 39, no. 3, pp. 880–901, 2001.

[50] G. Acosta and J. P. Borthagaray, "A fractional Laplace equation: regularity of solutions and finite element approximations," *SIAM Journal on Numerical Analysis*, vol. 55, no. 2, pp. 472–495, 2017.

[51] I. G. Graham, W. Hackbusch, and S. A. Sauter, "Finite elements on degenerate meshes: inverse-type inequalities and applications," *IMA Journal of Numerical Analysis*, vol. 25, pp. 379–407, Apr. 2005.

[52] H. Triebel, "Spaces of Besov-Hardy-Sobolev type on complete Riemannian manifolds," *Ark. Mat.*, vol. 24, pp. 299–337, 12 1985.

[53] J. L. Lions and E. Magenes, *Non-Homogeneous Boundary Value Problems and Applications*, vol. 1. Springer-Verlag, 1973.